Journal of Medicinal Chemistry

pubs.acs.org/jmc Article

Structure−Activity Studies of 3,9-Diazaspiro[5.5]undecane-Based γ-Aminobutyric Acid Type A Receptor Antagonists with Immunomodulatory Effect

Francesco Bavo, Heleen de-Jong, Jonas Petersen, Christina Birkedahl Falk-Petersen, Rebekka Löffler, Emma Sparrow, Frederik Rostrup, Jannik Nicklas Eliasen, Kristine S. Wilhelmsen, Kasper Barslund, Christoffer Bundgaard, Birgitte Nielsen, Uffe Kristiansen, Petrine Wellendorph, Yury Bogdanov, and Bente Frølund*

Cite This: https://doi.org/10.1021/acs.jmedchem.1c00290 Read Online

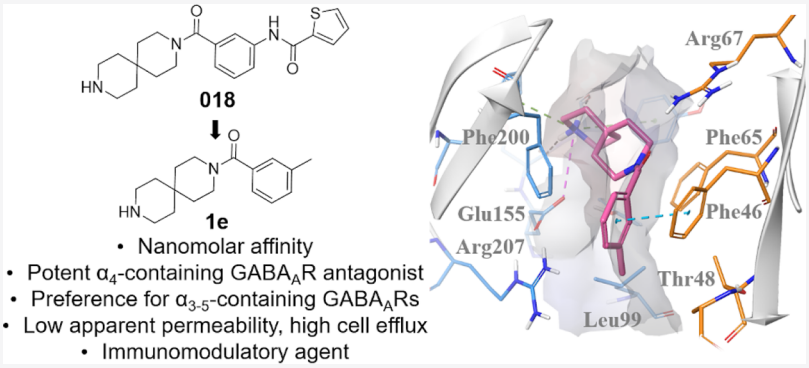

ABSTRACT: The 3,9-diazaspiro[5.5]undecane-based compounds **2027** and **018** have previously been reported to be potent competitive γ-aminobutyric acid type A receptor ($GABA_AR$) antagonists showing low cellular membrane permeability. Given the emerging peripheral application of $GABA_AR$ ligands, we hypothesize **2027** analogs as promising lead structures for peripheral $GABA_AR$ inhibition. We herein report a study on the structural determinants of **2027** in order to suggest a potential binding mode as a basis for rational design. The study identified the importance of the spirocyclic benzamide, compensating for the conventional acidic moiety for $GABA_AR$ ligands. The structurally simplified *m*-methylphenyl analog **1e** displayed binding affinity in the high-nanomolar range (K_i = 180 nM) and was superior to **2027** and **018** regarding selectivity for the extrasynaptic $\alpha_4\beta\delta$ subtype versus the α_1- and α_2- containing subtypes. Importantly, **1e** was shown to efficiently rescue inhibition of T cell proliferation, providing a platform to explore the immunomodulatory potential for this class of compounds.

■ INTRODUCTION

γ-Aminobutyric acid (GABA) is the major inhibitory neurotransmitter in the central nervous system (CNS) where it exerts the majority of its numerous functions through activation of ionotropic $GABA_A$ receptors ($GABA_ARs$) and metabotropic $GABA_B$ receptors.[1−3] Because of their involvement in a plethora of physiological and pathophysiological processes, modulation of neuronal $GABA_ARs$ holds considerable therapeutic potential.[4]

Recent studies have also identified an as yet unaddressed role of GABA in the peripheral organs.[5] In particular, a growing body of evidence emphasizes the importance of GABAergic signaling in the immune system. Indeed, GABA itself is produced by macrophages[6] and dendritic cells.[7] Various subunits of $GABA_AR$ have been identified in T cells,[8,9] monocytes,[8] macrophages,[6] and dendritic cells.[10] These data suggest that cells of the immune system possess a functional GABAergic system.

The function of GABA and the $GABA_ARs$ involved in the immune system is not well studied. However, it is currently accepted that GABAergic activation leads to immunosuppression. Indeed, administration of GABA to peritoneal macrophages leads to decreased proinflammatory cytokine production, while an increment was observed upon treatment with the $GABA_AR$ antagonist picrotoxin (PTX).[11] In addition, both

Received: February 15, 2021

PTX and the $GABA_AR$ agonist muscimol were shown to influence macrophage phenotype regulation.[6] Moreover, $GABA_AR$ activity seems to influence the ability of macrophages to fight infections.[12] Potentiation of $GABA_ARs$ activity through the positive allosteric modulator (PAM) alprazolam also has been shown to suppress T cell responses.[13] Indeed, $GABA_AR$ signaling negatively impacts T cell proliferation.[14] Knockout of the α_4 subunit of $GABA_ARs$ in a murine asthma model increases lung inflammation likely to be mediated by excessively active T cells.[15] Moreover, the δ subunit-selective $GABA_AR$ positive modulator DS2 shows anti-inflammatory activity in vitro and efficacy in ischemic stroke in vivo via a peripheral immune-related mechanism.[16]

The $GABA_ARs$ belong to the Cys-loop superfamily of ligand-gated ion channels, also comprising nicotinic acetylcholine receptors, 5-HT_3 receptors, and glycine receptors. The assembled receptor complex is a circular arrangement of five subunits making up a chloride selective ion-conducting channel. Nineteen different human $GABA_AR$ subunits have been identified; α_{1-6}, β_{1-3}, γ_{1-3}, δ, ε, θ, π, and ρ_{1-3}, and these subunits combine in different stoichiometries, the most common ones being 2α-2β-1γ heteropentamers.[17] The predominant combinations from the 26 native $GABA_AR$ subtypes proposed are believed to be $\alpha_1\beta_2\gamma_2$, $\alpha_2\beta_3\gamma_2$, and $\alpha_3\beta_3\gamma_2$.[1] The δ subunit is predominantly coassembled with α_4 or α_6 subunits into $\alpha\beta\delta$ receptors, mainly localized in extrasynaptic membranes, with high sensitivity to GABA and limited desensitization.[18] $GABA_ARs$ composed of ρ subunits assemble as homopentameric or pseudohomomeric receptors and are often referred to as $GABA_CRs$ since they are insensitive to classic $GABA_AR$ antagonists such as bicuculline (BCC).[19]

Since systemic administration of brain-permeant unspecific or subtype-unselective $GABA_AR$ antagonists (i.e., PTX or BCC) causes profound convulsant effects, they have been used as powerful tools to elucidate the physiological importance of the receptors without any therapeutic potential.[20] Indeed, although a number of $GABA_AR$ agonists or PAMs are approved for clinical use, the silent allosteric modulator flumazenil is the only $GABA_AR$ antagonist currently used in medical practice.[21] Due to the low number of $GABA_AR$ subtype-specific antagonists, the potential of such compounds as CNS targeting therapeutics has only been sparingly studied. Novel $GABA_AR$ antagonists with limited brain exposure and selectivity at the α_4- or δ- containing subtypes would be highly desirable tools for unraveling the role of $GABA_ARs$ in immunomodulation while contemporarily limiting the CNS related convulsant side effects, hence holding potential for in vivo applications.

Very few structural classes of competitive $GABA_AR$ antagonists exist,[22] exemplified by gabazine,[23] DPP-4-PIOL[24] and bicuculline (BCC)[25] (Figure 1). With the exception of BCC, orthosteric $GABA_AR$ antagonists contain both basic and acidic functionalities positioned in a narrow distance range from each other.[22] However, a novel class with mid to high nanomolar potency based on a 3,9-diazospiro[5.5]undecane moiety was recently identified in a compound library screening.[26] Unconventionally, neither the original hit **2027** nor the related analog **018** (Figure 1; here referred to as lead compounds), contain an acidic moiety. These compounds preferentially target $\alpha_{3/4/5}$-containing subtypes over $\alpha_{1/6}$ subtypes but do not differentiate between different β and γ/δ subunits. Importantly, in vitro permeability studies showed that **2027** and **018** do not passively cross MDCK-MDR1 cell membranes, thus making them less attractive for studying central $GABA_AR$ effects.[26] In contrast, **2027** and **018** are in fact more attractive as tools to investigate peripheral $GABA_AR$-mediated effects of GABA. Furthermore, sp^3-rich scaffolds and particularly spirocycles, such as diazaspiro[5.5]undecane, have recently attracted a lot of interest as unique platforms for modern drug design due to a general superiority of globular/spherical shaped molecules in binding to a defined target, selectivity and pharmacokinetic properties when compared with sp^2-rich flat molecules.[27,28] Owing to the inherent three-dimensionality and conformationally fixed structure, the spirocyclic scaffold is very well suited for probing the chemical space for $GABA_AR$-mediated effects.[29]

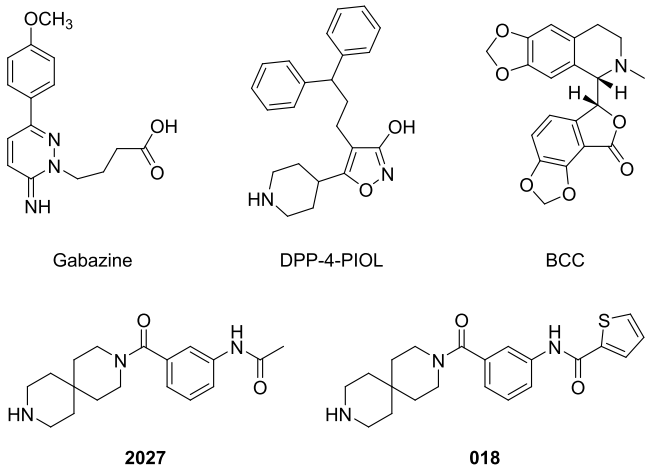

Figure 1. Chemical structures of gabazine, DPP-4-PIOL, BCC, and the 3,9-diazospiro[5.5]undecane analogs **2027** and **018**.

Inspired by the emerging peripheral applications of $GABA_AR$ antagonists and by the attractive physicochemical properties of the spirocyclic compounds in drug development, we have explored the spirocyclic **2027** as a lead structure for delineating the structural determinants for activity in order to suggest a potential binding mode as a basis for rational design and development with the overall aim of developing a α_4- and/or δ-selective $GABA_ARs$ antagonist with low brain exposure as a potential peripheral immunomodulator. We here report on the synthesis, pharmacological characterization and molecular modeling at the $GABA_AR$ of a series of compounds containing the spirocyclic scaffold as novel $GABA_AR$ antagonists. Finally, the potential for this class of compounds as effectors of T cell proliferation is evaluated.

RESULTS AND DISCUSSION

Design Strategy. Most conventional $GABA_AR$ ligands require an acidic group distanced approximately 5 Å from a basic center in order to interact with the conserved residue on the α subunit Arg 67 (α_1 subunit numbering) of the orthosteric binding pocket.[22,30,31] Both lead compounds considered in this study, **018** and **2027**, are lacking this feature but still maintain nanomolar binding affinity and nanomolar to submicromolar antagonist activity at the $\alpha_{3/4/5}\beta_{1/2}\delta/\gamma$ $GABA_AR$, respectively. Given the structural diversity of the novel chemical scaffold in the $GABA_AR$ area, we designed a SAR investigation aimed at unraveling structural components essential for binding at the $GABA_AR$ and feature(s) compensating for the absence of such a renowned pharmacophoric element, like acidic functionality.

https://doi.org/10.1021/acs.jmedchem.1c00290
J. Med. Chem. XXXX, XXX, XXX−XXX

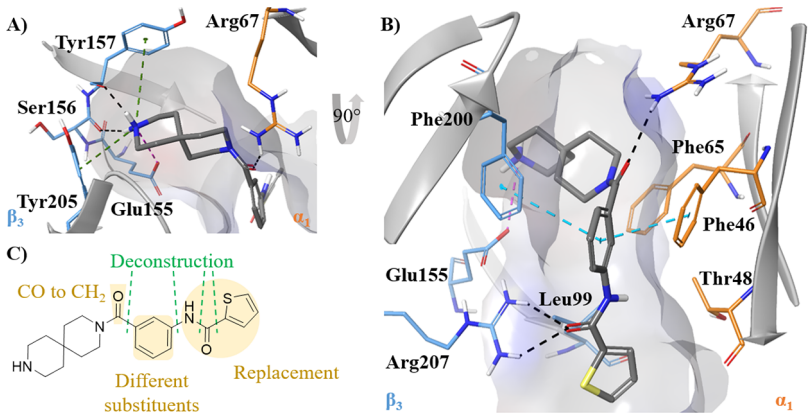

Figure 2. (A, B) Preliminary binding mode of **018** (dark gray) at the β_3/α_1 interface (PDB ID: 6HUK). The receptor backbone is shown in gray cartoons, while the carbons of relevant β_3 and α_1 residues are represented in light blue and orange, respectively. The inner surface of the receptor is shown in faded gray. Black dotted lines indicate H-bonds, magenta dotted lines represent electrostatic interactions, and green and cyan dotted lines respectively represent π−cation and π−π interactions. (C) Schematic overview of the design strategy: green dashed lines represent the disconnection points exploited for the progressive deconstruction of **018**, while moieties subjected to other modifications are highlighted in yellow.

Scheme 1. Synthesis of Amidated 3,9-Diazaspiro[5,5]undecane Analogs 1a−r[a]

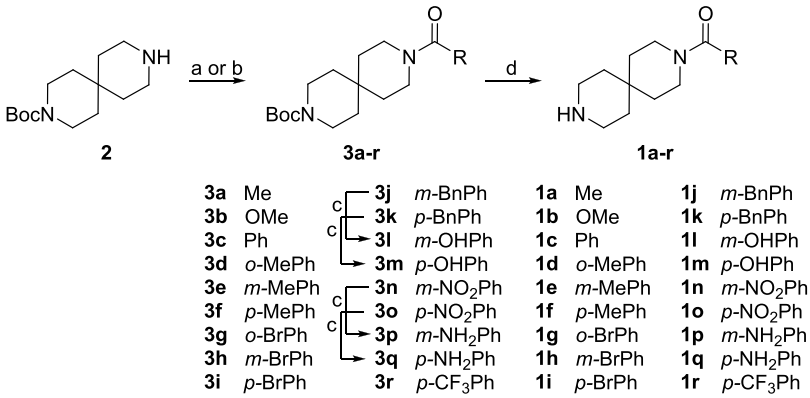

[a]Reagents and conditions. (a) RCOCl (for **3b−c** and **3n−o**) or $(RCO)_2O$ (for **3a** and **3r**), Et_3N, CH_2Cl_2, rt; (b) RCOOH, HBTU, Et_3N, CH_2Cl_2, rt (for **3d−k**); (c) H_2, Pd/C, EtOH, rt; (d) 4N HCl 1,4-dioxane in MeOH (for **1a−f**, **1 k−m**, **1o**, and **1q−r**) or CH_2Cl_2 (for **1j**, **1n**, and **1p**) or TFA in CH_2Cl_2 (for **1g−i**).

Preliminary molecular docking of **2027** and **018** at the orthosteric binding site of the $GABA_AR$, adapted from the recently reported cryo-EM structure of the $\alpha_1\beta_3\gamma_{2L}$ $GABA_AR$,[32] predicted the following interactions: (1) the positively charged spirocyclic secondary amine establishes an electrostatic interaction with β_3-Glu155, two H-bonds with the backbone carbonyls of β_3-Tyr 157 and β_3-Ser 156, and π−cation interactions with β_3-Tyr 205 and β_3-Tyr 97; (2) charge-assisted H-bond between the benzamidic carbonyl and α_1-Arg 67; (3) π−π interactions between the phenyl ring of **2027** or **018** and β_3-Phe 200 α_1-Phe 46; (4) charge-assisted H-bond between the acetamide of **2027** or the thienyl carboxamide of **018** and β_3-Arg 207; (5) Van der Waals interactions between the thienyl ring and β_3-Leu 99 and α_1-Thr 48 (Figure 2).

Due to the high degree of chemical modularity of **018** and **2027**, we envisioned that a progressive deconstruction approach would allow to test the preliminary binding mode and provide useful information about the role of each moiety, which could ultimately lead to a proposed binding mode. Based on extensive exploration of the spirocylic moiety of **2027**, a previous report[26] concluded that any modification to be detrimental for activity; hence, we focused on the *N*-substituent in the present study.

Assisted by molecular docking, we designed three series of analogs of **2027** and **018** (Figure 2). First, the extremely simplified analogs **1a,b** (Scheme 1) were designed to probe whether the spirocyclic tertiary amide alone could compensate the missing electrostatic interaction between α_1-Arg 67 and the acidic moiety, known pharmacophoric elements for the majority of $GABA_AR$ ligands, but not for **2027** and **018**. Second, the unsubstituted version of **2027** **1c** and its functionalized analogs **1d−r** (Scheme 1) were designed. Upon identification of two compounds with submicromolar affinity (**1e** and **1i**), their two amine analogs **1 s−t** (Scheme 2) were developed to address the joint effects of π−π stacking of the phenyl ring together with the H bonding of the spirocyclic amide. Last, compound **1u** was designed and developed as an amide-deficient methanolether analog of **018** (Scheme 3) to unravel the importance of the predicted H-bonding between the carboxamide of **018** and Arg 207.

Synthesis of Target Compounds. Compounds **1a−r** were synthesized according to Scheme 1. The commercially available building block *N*-Boc-3,9-diazaspiro[5,5]undecane (**2**) was acylated with acyl chlorides or anhydrides under basic conditions to obtain **3a−c**, **3n−o**, and **3r** or with carboxylic acids via a HBTU-mediated condensation reaction under basic

https://doi.org/10.1021/acs.jmedchem.1c00290
J. Med. Chem. XXXX, XXX, XXX−XXX

Scheme 2. Synthesis of Carbonyl-Deficient 3,9-Diazaspiro[5,5]undecane Analogs 1s and 1t[a]

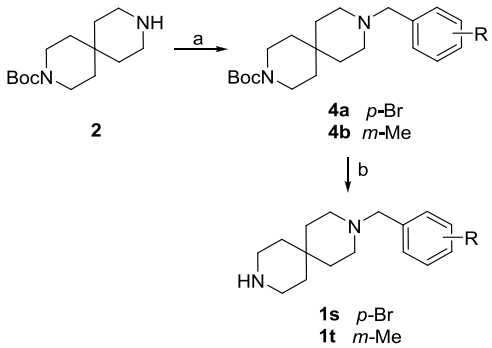

[a]Reagents and conditions. (a) RBnBr, Et_3N, CH_2Cl_2, rt; (b) TFA in CH_2Cl_2, rt (**1s**) or 4N HCl in 1,4 dioxane, CH_2Cl_2, rt (**1t**).

conditions to afford **3d−k**. Then, **3j−k** and **3n−o** were converted by catalytic Pd/C hydrogenolysis and hydrogenation to **3l−m** and to **3p−q**, respectively. The final compounds **1a−r** were achieved by deprotection of the Boc group under acidic conditions.

To further explore the SAR, two compounds lacking the carbonyl group, **1s** and **1t**, were prepared as illustrated in Scheme 2. The compounds were synthesized by the *N*-alkylation of **2** with the commercially available substituted benzyl bromides, yielding **4a** and **4b**. Deprotection of the Boc group under acidic conditions afforded **1s** and **1t**.

To further characterize the binding mode, a **018** analog deficient of thienyl amide was obtained via the convergent synthetic route depicted in Scheme 3. Intermediate **6** was synthesized by treating **5** with $SOCl_2$ to afford the alkyl chloride, followed by alkylation of methyl 3-hydroxybenzoate under basic conditions and subsequent deprotection of the methyl ester. A protecting group swap afforded intermediate **10** by treating **2** with trifluoroacetic anhydride under basic conditions and subsequent deprotection of the Boc group under acidic conditions. Intermediates **6** and **7** were coupled via HBTU-mediated condensation under basic conditions followed by deprotection of trifluoro acetamide to afford the final compound **1u**.

Structure−Affinity Relationship of the Target Compounds at the $GABA_A$Rs. The binding affinities of compounds **1a−u** at native $GABA_A$Rs were measured by [^{3}H]muscimol competition binding experiments to rat brain membrane preparations (Table 1). This binding assay utilizes a low concentration (5 nM) of [^{3}H]-muscimol and thus preferentially picks up binding to high-affinity extrasynaptic $GABA_A$Rs.[33]

The chemical modularity of the lead structure of **2027** prompted us to investigate the SAR by its progressive deconstruction into three different series of simplified analogs: **1a−b**, **1c−r**,**u** and **1s**,**t**. The extremely simplified *N*-acetyl 3,9-diazaspiro[5,5]undecane **1a** and its closely related analog **1b** displayed binding affinities in the mid−high micromolar range (37 and 100 μM, respectively), suggesting that the acetamide function alone is unable to compensate the absence of a carboxylic group. Compound **1a** was selected for further modification, gradually building the structure of **2027**: replacement of acetamide to benzamide provided compound **1c**, which exhibited more than 70 times improvement of binding affinity (K_i = 1.4 μM) compared to **1a**. The increase may be ascribed to additional lipophilic interactions with the receptor established by the aromatic ring, which is seemingly a pharmacophoric element of this scaffold. Then, electron-withdrawing or electron-donating substituents were introduced at the *o*-, *m*-, and *p*- positions of **1c**, providing the analogs **1d−r**. Whereas introduction of a methyl or a bromine at the *o*-position did not improve binding affinity (4.2 μM and 2.7 μM, respectively, for **1d** and **1g**), the same substituents at the *m*- and *p*- positions afforded compounds with high nanomolar affinity, ranging from 0.180 μM of **1e** (*m*-Me) to 0.52 μM of **1f** (*p*-Me). Furthermore, the *m*- and *p*- positions were probed either with polar substituents acting as hydrogen bond acceptors and/or donors, such as hydroxyl and amino groups, or with more lipophilic substituents, such as benzyloxy, nitro, and trifluoromethyl. The only compounds with slightly improved and submicromolar binding affinity (2 to 4 times) carried a polar and electron-donating substituent in the *m*- or *p*- position (0.34, 0.86, and 0.71 μM respectively for **1l**, **1m**, and **1q**). Conversely, none of the electron-withdrawing groups caused any affinity improvement and only provided similar or diminished binding affinities (9.4 μM for **1o**) compared to the unsubstituted parent compound **1c** (1.4 μM). Although no evident correlation between either the position or the nature of the substituent was detected, these two observations, taken together, could indicate a preference for compounds

Scheme 3. Synthesis of Amide-Deficient 018 Analog 1u[a]

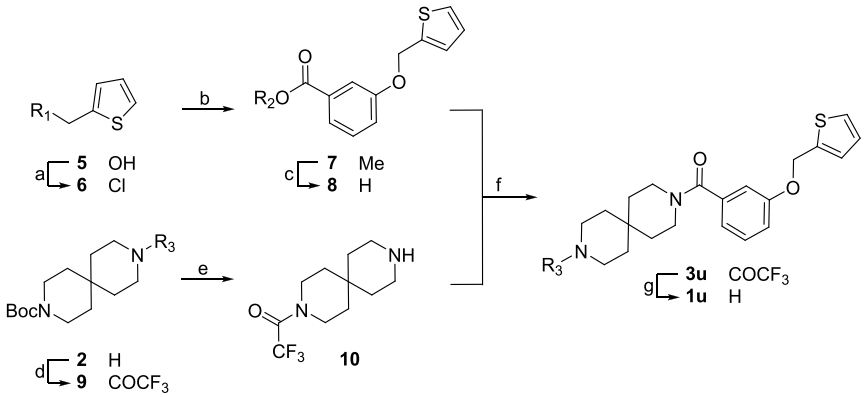

[a]Reagents and conditions. (a) $SOCl_2$ in CH_2Cl_2; (b) methyl 3-hydroxybenzoate, K_2CO_3, and DMF, 75 °C; (c) NaOH in THF:H_2O, rt; (d) TFAA, Et_3N, and CH_2Cl_2, 0 °C to rt; (e) 4N HCl in 1,4-dioxane in MeOH, rt; (f) HBTU, Et_3N, and CH_2Cl_2, rt; (g) 10% aq. NaOH in EtOH, rt.

https://doi.org/10.1021/acs.jmedchem.1c00290
J. Med. Chem. XXXX, XXX, XXX−XXX

Table 1. Pharmacological Data for 2027, 018, and the Synthesized Compounds 1a−t[a]

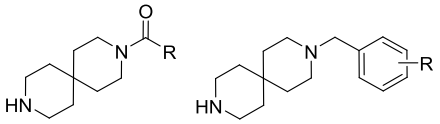

1a-r, u 1s-t

compound	R	[^{3}H]-muscimol-binding K_i (μM) (pK_i ± SEM)[b]
bicuculline[c]		4.57
gabazine[d]		0.074
2027[e]	*m*-acetamide	0.56
018[e]	*m*-(2-thienyl carboxamide)	0.020
1a	Me	>100
1b	MeO	37 [4.44 ± 0.06]
1c	Ph	1.4 [5.85 ± 0.02]
1d	*o*-Me-Ph	4.2 [5.38 ± 0.02]
1e	*m*-Me-Ph	0.18 [6.76 ± 0.05]
1f	*p*-Me-Ph	0.52 [6.30 ± 0.07]
1g	*o*-Br-Ph	2.7 [5.57 ± 0.04]
1h	*m*-Br-Ph	0.30 [6.55 ± 0.07]
1i	*p*-Br-Ph	0.23 [6.64 ± 0.01]
1j	*m*-BnO-Ph	1.0 [6.01 ± 0.09]
1k	*p*-BnO-Ph	1.0 [5.99 ± 0.05]
1l	*m*-OH-Ph	0.34 [6.49 ± 0.07]
1m	*p*-OH-Ph	0.86 [6.08 ± 0.07]
1n	*m*-NO_2-Ph	1.5 [5.83 ± 0.04]
1o	*p*-NO_2-Ph	9.4 [5.03 ± 0.04]
1p	*m*-NH_2-Ph	1.2 [5.93 ± 0.07]
1q	*p*-NH_2-Ph	0.71 [6.16 ± 0.08]
1r	*p*-CF_3-Ph	2.2 [5.66 ± 0.04]
1u	*m*-(2-thienyl methanol ether)	1.0 [6.00 ± 0.07]
1s	*p*-Br	27 [4.58 ± 0.04]
1t	*m*-Me	>200

[a]$GABA_A$R binding affinities at rat cortical synaptic membranes using [^{3}H]-muscimol. [b]IC_{50} values were extracted from the concentration−inhibition curves and converted into K_i values using the Cheng−Prusoff equation. The mean K_i values are given along with pK_i ± SEM values and are based on three independent experiments. [c]Measured at human $\alpha_1\beta_3\gamma_2$ $GABA_A$R stably expressed at Ltk cells. Data from Ebert et al.[34] [d]Data from Frølund et al.[35] [e]Data from Falk-Petersen et al.[26]

containing an electron-rich aromatic system. Whereas the *N*-acetylation of **1p** (1.2 μM) to the lead compound **2027** only slightly lowered the K_i to 0.53 μM, a 67× increase of binding affinity was observed through *N*-amidation to the 2-thienyl carboxamide analog **018**, suggesting the aromatic moiety to be responsible for improved binding. However, when we investigated the role of the amide group in the meta position by developing the *m*-thienylmethanol ether derivative **1u**, we observed 55× lower affinity than **018**, demonstrating that an aromatic moiety alone is not enough to obtain nanomolar binding affinity. This finding was confirmed by the micromolar affinity **1j** and **1k** and the benzylated analogs of **1l** and **1m**, respectively. Finally, we investigated the role of the tertiary amide at the spirocyclic moiety by synthesizing the amines **1s** and **1t**, which respectively showed 117× and more than 1000× reduced binding affinity when compared to their amidic analogs **1i** and **1e**. Altogether, the most high-affine analog identified was **1e** (K_i = 0.180 μM), albeit with 10× and 2× reduced affinity compared to **018** (K_i = 0.020 μM) and to the classical $GABA_A$R antagonist gabazine (K_i = 0.074 μM), respectively.[35,36]

Structural Rationalization of Major SAR Observations at $GABA_A$Rs. The most pronounced SAR effects are (1) a more than 70× increase in affinity by introducing a phenyl ring from **1a** into **1c**, (2) a more than 100× loss of affinity by replacing the spirocyclic tertiary amide of **1i** and **1e** to amine in **1s** and **1t**, and (3) a 67× increase in affinity by amidation of **1p** into the 2-thienyl carboxamide moiety of **018** compared to a modest 2× increase by acetylation, in opposition with a 55× decrease in affinity by replacing the primary amide of **018** with the hydroxymethyl of **1u**. To elucidate the molecular determinants underlying the SARs of these new unorthodox $GABA_A$R antagonists, we applied computational methods and performed a docking study of compounds **1a−u**, **2027**, and **018** at the orthosteric binding site of the extracellular β/α interface of $GABA_A$R. Most of the 3D structures of $GABA_A$Rs available are complexed with small agonist GABA (i.e., 6D6T), and are therefore more suitable for docking studies of agonists or small partial agonists.[30] Since antagonism is correlated with a more pronounced opening of the flexible loop C of the binding site, leading to more room for accommodating bulkier ligands,[32,37,38] we chose to use the β_3/α_1 interface from the recently reported cryo-EM of the human full-length $\alpha_1\beta_3\gamma_{2L}$ $GABA_A$R in complex with BCC (6HUK)[32] The BCC-bound orthosteric binding site represents a more realistic 3D model for docking of our novel spirocyclic antagonists, which share pharmacological activity (antagonists), size, and the lack of a carboxylic acid moiety with bicuculline (Figure S1). Since conventional $GABA_A$R ligands are based on the GABA scaffold, they contain a positively charged ammonium head appropriately distanced from a carboxylate, two renowned and essential pharmacophoric elements for $GABA_A$R recognition. Both at the β_2/α_1 and at the β_3/α_1 interfaces (PDB codes 6D6T and 6HUO, respectively)[30,32] the ammonium group of GABA (or its bioisosters) establishes an electrostatic interaction with β-Glu155 as well as $\pi-\pi$ interactions with the aromatic box formed by β-Y205 and β-Y200, while the carboxylate (or its bioisosters) forms electrostatic interactions with α_1-Arg 67 (Figure S2A).[39−41] Due to the high degree of similarity among subunits within the orthosteric binding pocket, the corresponding residues at the other subunits are conserved (β_1 compared to β_2 and β_3 and α_2, α_3, α_4, α_5, and α_6 compared to α_1).[30,42] Although all the hereby reported compounds do not have any carboxylic function and therefore miss an interaction believed to be essential for high affinity $GABA_A$R binding, some of them reach nM affinities, meaning that one or more of the other chemical features compensate for the lack of the carboxylic group.

*Aromatic Ring of **1a** Enables Access to a Lipophilic Subpocket.* Comparing the binding poses of **1a** and **1c** (Figure 3) provides a qualitative explanation of the 70-fold difference in affinity. Both ammonium groups establish electrostatic interactions with β_3-Glu 155, H-bonds with the carbonyl backbones of β_3-Ser 156 and β_3-Tyr 157, and π−cation interactions with β_3-Tyr 205 and β_3-Tyr 157 of the aromatic cage. Whereas both amidic carbonyls of **1a** and **1c** are predicted to H-bond Arg 67, the phenyl ring of **1c** is sandwiched between β_3-Phe 200 (located on loop C) and α_1-Phe 46, with which it establishes face-to-edge and face-to-face $\pi-\pi$ stacking, respectively. A similar interaction pattern can be observed in the original cryo-EM complex 6HUK, where the benzodioxole moiety of bicuculline interacts with β_3-Phe 200

https://doi.org/10.1021/acs.jmedchem.1c00290
J. Med. Chem. XXXX, XXX, XXX−XXX

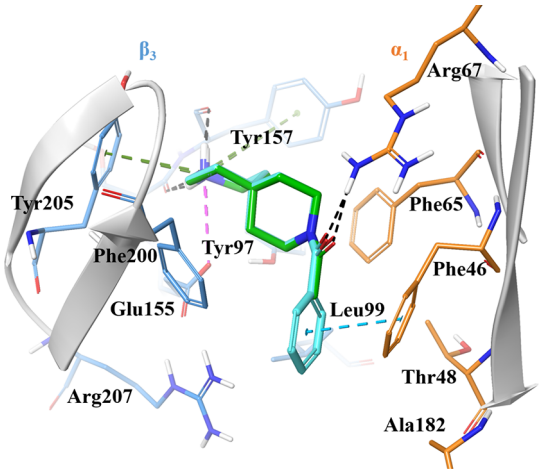

Figure 3. Binding mode of **1a** (green) and **1c** (cyan) as representative of carboxylic-deficient $GABA_AR$ ligands by docking at the β_3/α_1 interface (PDB ID: 6HUK). Receptor backbone is shown in gray cartoons, while the carbons of relevant β_3 and α_1 residues are represented in light blue and orange, respectively. Black dotted lines indicate H-bonds, magenta dotted lines represent electrostatic interactions, and green and cyan dotted lines respectively represent π−cation and π−π interactions. The more potent **1c** establishes additional π−π interactions with Phe 200 and Phe 46 as compared to **1a**.

by π−π stacking (Figure S1), and has been hypothesized to be relevant for binding of bulky $GABA_AR$ antagonists based on the scaffolds of 5-(4-piperidyl)-3-isoxazolol (4-PIOL) or 4-(4-piperidyl)-1-hydroxypyrazole (4-PHP).[43−47] By distancing the loop C from the α_1 subunit, the phenyl ring seems to grant access to a lipophilic cavity lined by β_3-Leu 99, α_1-Thr 48, α_1-Ala 182, and β_3-Arg 207 located toward the transmembrane domain. The subpocket is normally not accessible in GABA-bound 3D models because the flexible loop C is tightly closed onto the agonist and keeps β_3-Phe 200 in proximity with α_1-Phe 46 and α_1-Phe 65, occluding access to the subpocket (Figure S2A).[30,32] The opening of a corresponding subpocket has been observed in acetylcholine binding proteins (AChBP), a soluble surrogate of Cys-loop receptors.[37,48] Moreover, β-Leu 99 and β-Arg 207 have been reported to line the orthosteric binding site and to be involved in channel gating.[49,50] Compounds **1d−i** and **1l−r** are predicted to bind similarly to **1c**, with the exception of the substituent directionality: whereas *m*- substituents of **1e**, **1h**, **1l**, **1n**, and **1p** are projected toward β_3-Leu 99, with which apolar functional groups such as methyl (**1e**) or bromine (**1h**) can establish lipophilic contacts, *p*- substituents of **1f**, **1i**, **1m**, **1o**, **1q**, and **1r** are placed between α_1-Ala 182 and β_3-Arg 207, pointing toward the outer region of the binding pocket (Figure S3).

The Spirocyclic Benzamide Is Important for Affinity. Lack of affinity of **1a** and micromolar K_i of **1c** would suggest that the phenyl ring, but not the tertiary amide, is important for binding. However, since the amide of all compounds is predicted to hydrogen-bond to α_1-Arg 67, we designed and synthesized **1s** and **1t** as amine analogs of **1i** and **1e**, respectively. They both turned out to be devoid of affinity, suggesting that the carbonyl might interact with α_1-Arg 67. In addition, **1s** and **1t** are predicted to exist in their dicationic protonation state at physiological pH. According to the docking, the resulting tertiary ammonium group should be unconventionally placed between two positively charged arginines, α_1-Arg 67 and β_3-Arg 207, and would therefore be subjected to repulsive forces that impair binding (Figure 4).

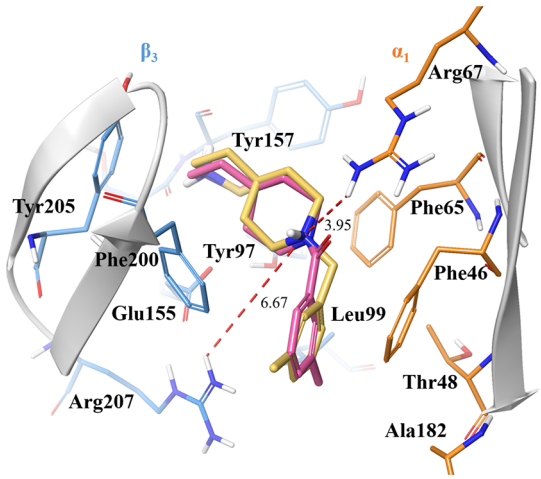

Figure 4. Comparison between the binding modes of **1e** (pink) and **1t** (yellow), predicted by docking at the β_3/α_1 interface (PDB ID: 6HUK). The red dashed lines represent unfavorable ligand-residue distances due to electrostatic repulsions between the positively charged tertiary amine of **1t** and the positively charged Arg 207 and Arg 67. For sake of clarity, the H-bond between the amidic carbonyl of **1e** and Arg 67 is not shown.

*High Affinity of **018** Can Be Related to Additional Interactions in the Lipophilic Pocket.* The binding poses of **2027** and **018** provide an explanation for their improved binding affinities when compared to their common precursor **1p**. In both cases, the newly introduced secondary amide interacts through a bidentate H-bond with β_3-Arg 207. Moreover, the lipophilic 2-thienyl group of **018** is placed in the abovementioned lipophilic subpocket and makes extensive Van der Waals contact with β_3-Leu 99. To further investigate the role of the amide/β_3-Arg 207 interaction, we designed the thienylmethanol ether analog **1t** and its benzyloxy derivatives **1j** and **1k**. Their 55-fold lower affinities suggest that the secondary amide is crucial for high affinity, either by H-bonding β_3-Arg 207 or by keeping the structure planar and rigid, so that the thiophene faces the side chain of β_3-Leu 99 (Figure 5).

Antagonistic Potency and Subtype Profiling of 1e and 1f. To assess the effect on subtype selectivity of the structural modifications performed, the functional profile at selected $GABA_AR$ subtype combinations of the compound with highest binding affinity of the series **1e** and its closely related analog **1f** were explored using a fluorescence-based FLIPR membrane potential (FMP) assay (Table 2). Reflecting the measured binding affinities, **1e** displayed higher antagonist potency than **1f** at all tested receptor subtypes. As reported for **2027** and **018**,[26] the potencies of **1e** and **1f** were highly dependent on the specific α subunit. As depicted in Table 2, both **1e** and **1f** showed preference for the α_{3-5}-containing receptors with potencies in the high nanomolar range (195−560 nM), whereas the potency at $\alpha_{1,2,6}$-containing receptors were in the low micromolar range (1.95−7.56 μM), confirming the trend observed for **2027** and **018**. Overall, a similar trend for potency ranking based on α-subunit, $\alpha_4 > \alpha_5 = \alpha_3 > \alpha_6 > \alpha_1 > \alpha_2$, was seen for **1e** and **1f** as reported for **2027** and **018**,[26] indicating a preference for the extrasynaptic $GABA_ARs$, often

https://doi.org/10.1021/acs.jmedchem.1c00290
J. Med. Chem. XXXX, XXX, XXX−XXX

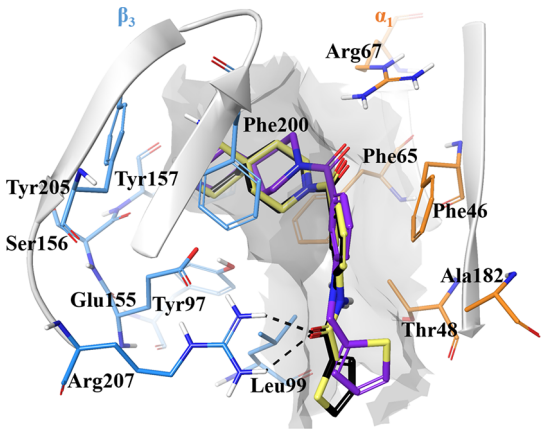

Figure 5. Binding mode of **1t** (purple), **2027** (yellow), and **018** (black) by docking at the β_3/α_1 interface (PDB ID: 6HUK). Black dashed lines represent bidentate H-bonds, while the inner surface receptor is depicted in faded gray.

containing α_4 but not limited hereto, in contrast to the classical nonselective antagonist gabazine (IC_{50s} = 0.11, 0.24, and 0.24 μM at $\alpha_4\beta_1\gamma_2$, $\alpha_4\beta_1\delta$, and $\alpha_1\beta_2\gamma_2$ respectively).[26,35,36]

Of utmost importance, **1e** was not only five times more potent than **2027** but also markedly more selective than both **2027** and **018** for the $\alpha_4\beta_1\delta$ subtype versus the α_1- (67 times) and α_2- containing (129 times) subtypes (vs 2−10 times for the lead compounds).

Functional Selectivity and Dissociation Kinetics of 1e. In order to confirm the selectivity of **1e** for $\alpha_4\beta_1\delta$ receptors over $\alpha_1\beta_2\delta$ receptors observed in the FMP assay and to obtain kinetic information about the interaction of **1e** with these receptors, we performed whole-cell patch-clamp experiments with the same kind of transfected cells as used in the FMP assay. The results of this are summarized in Figure 6 and detailed in Figure S4.

Application of GABA at a concentration eliciting a near maximal response (EC_{90-100}) gave rise to a fast-activating outward current with a time constant for activation of τ = 43 ms [35; 52] and τ = 38 ms [33;52] (median and interquartile interval) for the $\alpha_4\beta_1\delta$ (100 μM GABA) and $\alpha_1\beta_2\delta$ receptors (1 mM GABA), respectively. With $\alpha_4\beta_1\delta$ receptors, preapplication of the antagonist **1e** in increasing concentrations gave rise to a gradual replacement of this fast component of activation with a slow component (Figure 6A and Figure S4A) and, thus, a decrease of the fractional amplitude of the fast component ($\%A_{fast}$) from 100 to 0% (Figure 6B and Figure S4B), as observed previously for the slowly dissociating $GABA_A$ antagonist **018** on these receptors.[26] In line with (and as detailed in) that study, we interpret the fast and slow

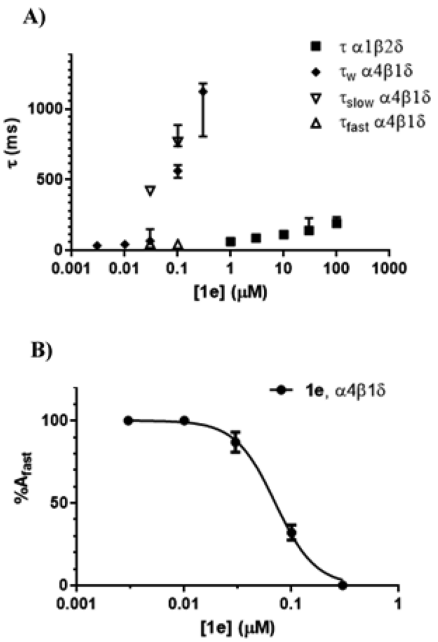

Figure 6. (A) Activation time constants, τ, for currents induced by GABA (EC_{90-100}) with preapplication of varying concentrations of **1e** on $\alpha_1\beta_2\delta$ and $\alpha_4\beta_1\delta$ receptors measured by whole-cell patch-clamp recording. τ values were determined by monoexponential curve fitting except for 0.03 and 0.1 μM **1e** on $\alpha_4\beta_1\delta$ receptors, where a slow and fast phase of receptor activation could be resolved by biexponential curve fitting resulting in τ_{fast} and τ_{slow}, respectively (open symbols). For the $\alpha_4\beta_1\delta$ receptor, a weighted τ value (τ_w) is shown. This is a weighted average of the τ_{fast} and τ_{slow} values, weighted by their fractional contribution to the total current amplitude. For the concentrations where monoexponential fitting was used, τ_w is just the single τ values obtained. Data are shown as median ± interquartile range for 4−12 cells. (B) The fractional contribution of the fast components of receptor activation to the total current amplitude ($\%A_{fast}$) decreases as a function of the concentration of **1e** on $\alpha_4\beta_1\delta$ receptors. $\%A_{fast}$ represents the fraction of receptors not occupied by **1e** at the end of the 20 s preapplication just before GABA is applied. Data are shown as mean ± SEM or 4−12 cells. The concentration of **1e** corresponding to $50\%A_{fast}$ was estimated by curve fitting to 71 nM (pIC_{50} ± SEM = 7.152 ± 0.029).

Table 2. Antagonist Activity of 1e, 1f, 2027, and 018 at Selected Subtypes[a]

	IC_{50} (uM) (pIC_{50} ± SEM; n = 3)[b]			
	1e	**1f**	**2027**[c]	**018**[c]
$\alpha_1\beta_2\delta$	4.95 (5.31 ± 0.037)	13.2 (4.88 ± 0.019)	6.68 (5.17 ± 0.10)	0.24 (6.61 ± 0.050)
$\alpha_4\beta_1\delta$	0.195 (6.74 ± 0.11)	1.28 (5.90 ± 0.052)	1.03 (5.99 ± 0.028)	0.088 (5.99 ± 0.028)
$\alpha_4\beta_2\delta$	0.250 (6.60 ± 0.023)	2.15 (5.67 ± 0.031)	0.36 (6.44 ± 0.12)	0.068 (7.17 ± 0.080)
$\alpha_6\beta_2\delta$	1.95 (5.72 ± 0.058)	8.87 (5.06 ± 0.092)	4.13 (5.38 ± 0.05)	0.33 (6.48 ± 0.082)
$\alpha_1\beta_2\gamma_2$	2.18 (5.66 ± 0.026)	10.0 (5.00 ± 0.018)	4.96 (5.30 ± 0.17)	0.79 (6.10 ± 0.11)
$\alpha_2\beta_2\gamma_2$	7.56 (5.13 ± 0.047)	25.3 (4.60 ± 0.052)	2.96 (5.53 ± 0.19)	0.32 (6.49 ± 0.13)
$\alpha_3\beta_2\gamma_2$	0.56 (6.30 ± 0.13)	3.57 (5.49 ± 0.12)	0.29 (6.54 ± 0.17)	0.079 (7.10 ± 0.18)
$\alpha_5\beta_2\gamma_2$	0.54 (6.27 ± 0.052)	1.50 (5.84 ± 0.074)	0.59 (6.23 ± 0.19)	0.051 (7.29 ± 0.19)

[a]Functional characterization at selected human $GABA_AR$ receptors transiently expressed in HEK293 cells using the FMP assay. [b]The mean IC_{50} values are given along with pIC_{50} ± SEM values and are based on at least three independent experiments using GABA EC_{80} as agonist concentration. [c]Data from Falk-Petersen et al.[26]

https://doi.org/10.1021/acs.jmedchem.1c00290
J. Med. Chem. XXXX, XXX, XXX−XXX

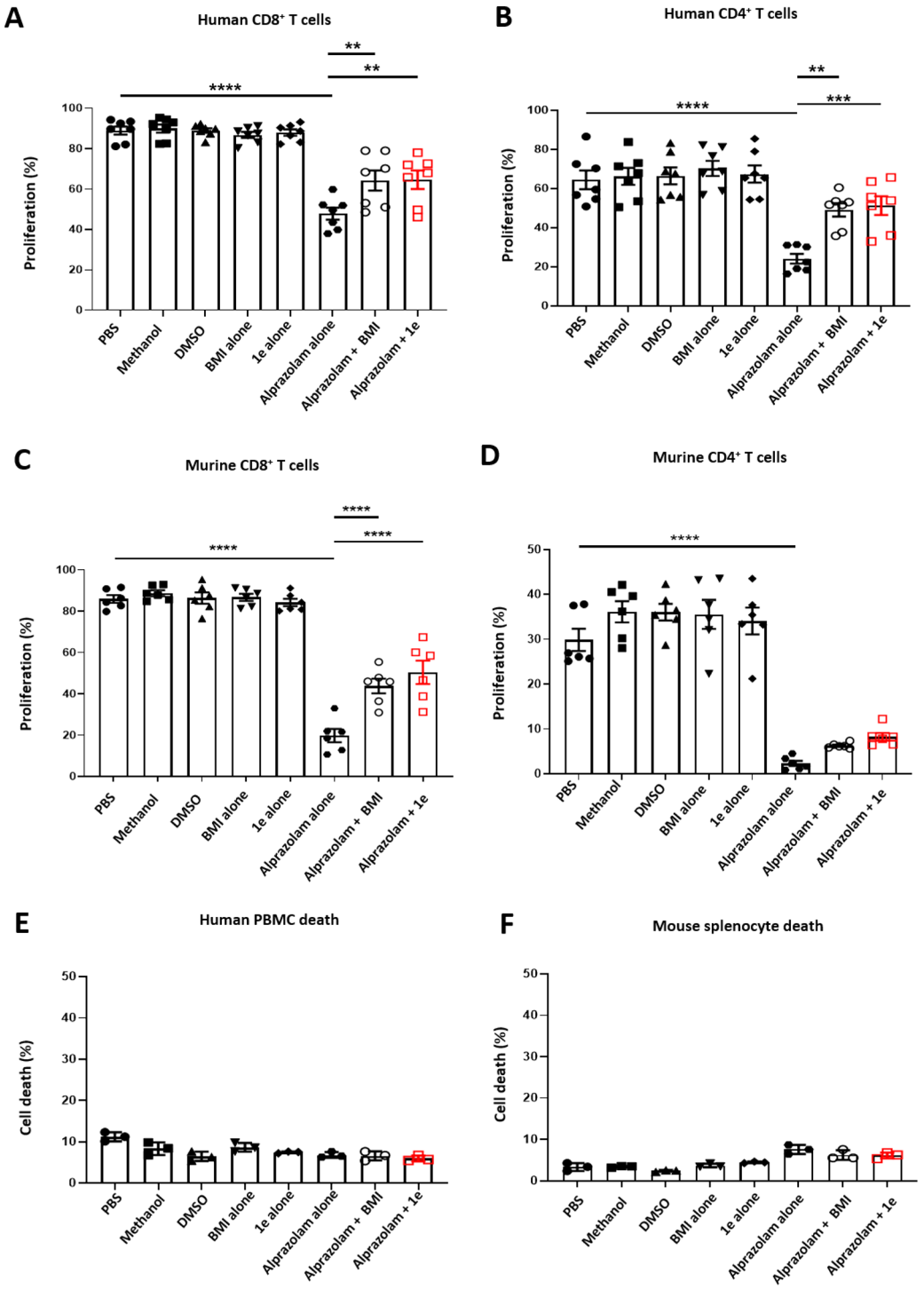

Figure 7. 1e rescues inhibition of proliferation induced by alprazolam in both human PBMC (A, B) and mouse splenocytes (C, D) populations with minimal cell toxicity (E, F). Cells were stained with CFSE (5 μM) and stimulated with soluble α-CD3 antibody (33 ng/mL for splenocytes and 100 pg/mL for PBMC) in order to induce T cell proliferation (PBS control). Alprazolam (33 μM for PBMC and 100 μM for splenocytes) inhibits α-CD3-induced proliferation, while BMI (100 μM) and **1e** (50 μM) recover inhibition of proliferation induced by alprazolam. As methanol is used to reconstitute alprazolam and DMSO used to reconstitute **1e**, these were included as controls. Data shown is a combination of at least six independent experiments, and error bars show standard error of the mean (SEM). Statistical significance was determined by one-way ANOVA with Tukey's multiple comparison test. $^{**}P < 0.01$. $^{***}P < 0.001$. $^{****}P < 0.0001$.

components as GABA interacting with two "populations" of receptors: those that are initially vacant (and therefore immediately available for GABA to bind to and activate) and those that are initially occupied with antagonist, where GABA activation has to await **1e** to dissociate from the receptor, which is the rate-limiting step. Accordingly, the time constant of the slow component of activation, τ_{slow}, is interpreted as reflecting the antagonist dissociation rate, and $\%A_{fast}$ as the proportion of receptors not occupied by antagonist at the onset of GABA application. Provided that the antagonist

https://doi.org/10.1021/acs.jmedchem.1c00290
J. Med. Chem. XXXX, XXX, XXX−XXX

binding has reached equilibrium at the end of the preapplication, the concentration dependence of $\%A_{fast}$ allows us to estimate the antagonist concentration resulting in 50% $A_{fast,}$ corresponding to 50% equilibrium receptor occupation by **1e**, i.e., a "functional" K_B. This was found to be 71 nM (7.152 ± 0.029), which is approximatey 10-fold higher than the K_B as previously obtained for **018** in a similar way (6.9 nM).[26]

The τ obtained with 0.3 μM **1e** on $\alpha_4\beta_1\delta$ receptors (where $\%A_{fast} = 0$) represents the situation where all receptors are occupied by **1e** at the time where GABA is applied, and thus, the corresponding τ value (1.12 s [0.81; 1.18]) reflects the dissociation rate of **1e** from the receptors. This value is appoximately 3-fold faster than the corresponding τ previously obtained for **018** (3.7 s [2.7;4.3])[26] and suggests that the decrease in potency from **018** to **1e** is partly due to the increased dissociation rate constant ($=1/\tau$).

With $\alpha_1\beta_2\delta$, receptors the results were less clear-cut. It was not possible to resolve the fast and slow components of receptor activation at any concentration. This is likely due to the τ value for dissociation of **1e** from the $\alpha_1\beta_2\delta$ receptor being faster and therefore closer to the τ_{fast} for GABA activation of the vacant receptor. The τ values for **1e** from the $\alpha_1\beta_2\delta$ receptor obtained from monoexponantial curve fitting are thus hybrids of the underlying τ_{fast} and τ_{slow}, where the contribution of τ_{fast} decreases with increasing concentration of **1e** and the hybrid τ value increases accordingly with higher concentrations of **1e** (in a similar way as the weighted time constant τ_w for $\alpha_4\beta_1\delta$ receptors). It is apparent from Figure 6A and Figure S4A that at the $\alpha_1\beta_2\delta$ receptor, considerably higher concentrations of **1e** are required to associate to the receptor and increase the τ value over the value from GABA activation of the vacant receptor, confirming the lower potency of **1e** on $\alpha_1\beta_2\delta$ receptors that was observed in the FMP assay. Furthermore, the τ value obtained with highest concentration of **1e** (189 ms [176; 235]) is (approximately 6-fold) faster than for the $\alpha_4\beta_1\delta$ receptor. Thus, the lower potency observed on $\alpha_1\beta_2\delta$ receptors , which correlates well with the results from the FMP assay, is partly due to a faster dissociation rate constant from the receptor.

Membrane Transport Characteristics of 1e. The membrane transport characteristics of **1e** were examined in vitro across cell monolayers of MDCK-MDR1 cells. The bidirectional transport was measured following addition of the test compound (0.5 μM) to the apical or basal side of the cell layer. **1e** was found to have low apparent apical to basal permeability ($1.3 \pm 0.19 \times 10^{-6}$ cm/s), whereas the basal to apical transport rate was substantially higher ($15 \pm 1.0 \times 10^{-6}$ cm/s). The resultant efflux ratio of 11.5 indicates that **1e** is a strong P-gp substrate and thus has a low likelihood of being distributed to the central nervous system following systemic dosing in vivo.

The pharmacological profile, combined with a simplified structure compared to **018** and the low likelihood of reaching the CNS, prompted us to further investigate **1e** as a potential immunomodulatory agent.

Rescue of T Cell Proliferation. As discussed above, it has been shown that stimulation of $GABA_A$Rs leads to inhibition of many T cell functions, including proliferation.[14] With this in mind, we investigated the ability of **1e** (50 μM) to rescue proliferation inhibited by GABAergic signaling and compared this with the rescue seen on treatment with the classical $GABA_A$R antagonist bicuculline methiode (BMI). We tested **1e** on both human PBMC and mouse splenocytes in a proliferation assay format.

Cells were stimulated with anti-CD3 antibody in order to induce T cell proliferation used as a positive control. Benzodiazepine alprazolam was used as a positive allosteric modulator of $GABA_A$Rs, inducing decrease of proliferation, and **1e** or BMI was added to alprazolam-treated cells in order to observe rescue of proliferation. Flow cytometry was used to determine the percentage of $CD8^+$ and $CD4^+$ T cells proliferating under each experimental condition (Figure S5).

Treatment of human $CD8^+$ T cells with anti-CD3 antibody resulted in an average of 78.9 ± 13.5% proliferation after 96 h of culturing (Figure 7A). $CD4^+$ T cell populations proliferated slightly less efficiently, with an average proliferation of 59.8 ± 19.6% (Figure 7B). However, in both cell populations, the addition of alprazolam led to a statistically significant decrease in proliferation, which was similar in both cell populations tested (34.8 and 35.7% for $CD8^+$ and $CD4^+$ T cells, respectively). Addition of BMI was able to partially rescue proliferation by approximately 20% in both cell populations. The addition of **1e** to cells treated with alprazolam also led to a 20% significant recovery of proliferation in both $CD8^+$ and $CD4^+$ T cell populations. Interestingly, however, this amount of rescue was achieved at a lower concentration of 50 μM **1e** as compared to 100 μM BMI, suggesting that **1e** is able to inhibit $GABA_A$Rs more efficiently.

We also determined the ability of **1e** to rescue proliferation in mouse $CD8^+$ and $CD4^+$ T cell populations (Figure 7C,D). We observed a similar trend to that seen in human T cell populations. In both cell populations, there was a substantial reduction in proliferation in response to alprazolam treatment, which was determined to be statistically significant. As with human T cell populations, we were able to observe a marked increase in proliferation when alprazolam-treated cells were additionally treated with either BMI or **1e**. Again, **1e** appeared to be the more efficient $GABA_A$R antagonist and was in fact able to rescue proliferation in slightly more cells in both populations with minimal cell toxicity (Figure 7E,F) despite the lower concentration used compared to BMI.

To exploit potential off-target mediated effects in the T cell proliferation assay, **1e** (50 μM) was subjected to a screening campaign against a selection of targets, including enzymes and transporters involved in the catabolism and reuptake of GABA, ion channels belonging to the class of Cys-loop receptors, and GPCRs expressed in T-cells.

1e was shown to be inactive at human GABA transporters (GAT1, GAT2, BGT1, GAT3) at the GABA transaminase, and no significant binding to $5HT_1B$, $5HT_2B$ and $5HT_7$ receptors was detected (Figure S6). Although at the high concentration tested, **1e** moderately binds to the α7 nACh and to the 5-HT3 receptors, these are only faintly expressed in T cells according to various databases (https://immgen.org, http://biogps.org, http://proteinatlas.org).[51] This information, combined with the high expression levels of $GABA_A$Rs in T cells,[52] the high $GABA_A$R potency of **1e**, and a very specific antiproliferative effect induced by benzodiazepine alprazolam reverted by two chemically diverse $GABA_A$Rs antagonists **1e** and BMI, strongly suggests a $GABA_A$R-mediated effect of **1e**.

■ CONCLUSIONS

In summary, we have expanded the pool of $GABA_A$R ligands based on the unconventional $GABA_A$R antagonists **2027** and **018**, all characterized by the spirocyclic scaffold and the lack of

https://doi.org/10.1021/acs.jmedchem.1c00290
J. Med. Chem. XXXX, XXX, XXX−XXX

an acidic moiety. The combination of the analysis of the structure affinity relationships, together with molecular docking, allowed us to propose a binding mode for **2027** and analogs that well interprets the affinity data, offering a platform to exploit the spirocyclic scaffold for exploring the chemical space. Micromolar affinity can only be achieved by benzamidation of the spirocyclic scaffold, probably to provide an appropriate H-bonding partner for Arg 67 and productive $\pi-\pi$ interactions with Phe 200 and Phe 46. Further increases in affinity by *m*-amidation of the phenyl ring can be ascribed to H-bonding to Arg 207 accompanied by additional lipophilic contact with a rather inaccessible lipophilic cavity. The compound with highest binding affinity (**1e**) displayed antagonist functional activity in the FMP assay and patch-clamp electrophysiology, with preference for α_{3-5} containing receptors and reaching the highest potency at the α_4-containing receptors. Functional activity of **1e** as an immunomodulatory agent was evaluated, and it was found to be superior to the known commercial $GABA_AR$ antagonist BMI in rescuing proliferation of T cells pretreated with alprazolam, a $GABA_AR$-positive allosteric modulator that inhibits T cell proliferation.

All in all, these results, together with the low apparent membrane permeability, high potency, and overall selectivity of **1e** and preference for α_{3-5}-containing $GABA_ARs$, provide the tools for rational design and development of further peripheral unconventional $GABA_AR$ antagonists with immunomodulatory activity.

■ EXPERIMENTAL SECTION

Chemistry. *General Procedures.* All reagents and materials were purchased from commercial suppliers and used without further purification. The solvents used were of standard HPLC-grade quality. Anhydrous THF, CH_2Cl_2, and DMF were obtained from a Glass Contour Solvent System (SG Water USA).

Anhydrous MeOH was obtained by storage over activated 3 Å molecular sieves for a minimum of 24 h (according to standard protocols). Et_3N and pyridine were kept dry by storage over KOH pellets. For thin-layer chromatography (TLC), Merck aluminum sheets covered with silica gel C-60 F_{254} were used and visualized using UV light (254 nm) or $KMnO_4$. Flash chromatography was performed using glass columns packed with Merck Geduran Si 60 (0.040−0.063 mm) as a stationary phase. Eluent systems are specified for each R_f value and reported as volume ratios. The eluent systems for flash chromatography is specified under each protocol.

1D and 2D NMR spectra were acquired using a Bruker Avance II equipped with a 5 mm broad band probe (BBFO) operating at 400 MHz for ^{1}H NMR and 101 MHz for ^{13}C NMR or a Bruker Avance III HD equipped with a cryogenically cooled 5 mm dual probe optimized for ^{13}C and ^{1}H NMR operating at 600 MHz for ^{1}H NMR and 151 MHz for ^{13}C NMR. HSQC, HMBC, H2BC, NOESY, and HSQC-TOCSY experiments were used to support analyses when ^{1}H NMR, ^{13}C NMR, and COSY were inadequate. Chemical shifts (δ) are reported in ppm downfield from TMS (δ = 0) using solvent resonance as the internal standard (chloroform-*d*, ^{1}H: 7.26 ppm, ^{13}C: 77.16 ppm; dimethylsulfoxide-d_6 , ^{1}H: 2.50 ppm, ^{13}C: 39.52 ppm; methanol-d_1, ^{1}H: 3.31 ppm, ^{13}C: 49.00 ppm; D_2O, ^{1}H: 4.79 ppm). Coupling constants (*J*) are reported in Hz, and the field is reported in each case. Multiplicities are reported as singlet (s), broad singlet (br. s), doublet (d), doublet of doublets (dd), doublet of triplets (dt), doublet of doublet of doublets (ddd), doublet of doublet of triplets (ddt), triplet (t), triplet of doublets (td), quartet (q), pentet (p), septet (sep), and multiplet (m).

Mass spectrometric data was recorded using either a LC-MS system built from an Agilent 1200 series solvent delivery system equipped with an autoinjector coupled to a DAD and an Agilent 6130A series quadrupole electrospray ionization detector or a Waters Aquity UPLC-MS equipped with a dual-wavelength PDA (214 and 254 nm) combined with electrospray ionization. Gradients of H_2O/MeCN/HCOOH (95:5:0.1) (solvent A) and MeCN/HCOOH (100:0.1) (solvent B) were employed.

Purity was assessed by analytical HPLC on an UltiMate HPLC system (Thermo Scientific) consisting of an LPG-3400A pump (1 mL/min), a WPS-3000SL autosampler, and a DAD-3000D diode array detector using a Gemini-NX C18 column (4.6 × 250 mm, 3 μm, 110 Å); gradient elution was 0 to 100% B (MeCN/H2O/TFA, 90:10:0.1) in solvent A (H2O/TFA, 100:0.1) over 15−20 min. Data were acquired and processed using Chromeleon Software v. 6.80. Analytical purity is ≥95% unless stated otherwise; retention times (t_R) are indicated.

Preparative HPLC purification was carried out on a Dionex Ultimate 3000 HLPC system consisting of an LPG-3200BX pump (20 mL/min), a Rheodyne 9725i injector, a 10 mL loop, an MWD-3000SD detector (200, 210, 254, and 281 nm), and an AFC-3000SD automated fraction collector using a Gemini-NX C18 column (21.2 × 250 mm, 5 μm, 110 Å); gradient elution was 0 to 80% B (MeCN/H2O/TFA, 90:10:0.1) in solvent A (H2O/TFA, 100:0.1) over 12 min. Data were acquired and processed using Chromeleon Software v. 6.80.

*Method A: Preparation of Compounds **3a−c, 3n−o,** and **3r**.* In a Schlenk dry round-bottomed flask equipped with a magnetic stirring bar, *tert*-butyl 3,9-diazaspiro[5.5]undecane-3-carboxylate **2** (1.2 mmol, 1 eq) and dry Et_3N (2 or 3 eq) were dissolved in dry CH_2Cl_2 (20 mL), and the solution was cooled at 0 °C before dropwise addition of the appropriate acyl anhydride or acyl chloride (from 1.2 to 1.5 eq). The reaction was stirred at rt for 2 h, quenched by addition of aqueous HCl (1N, 30 mL) and transferred to a separatory funnel with CH_2Cl_2 (25 mL). The organic layer was separated and washed with saturated aqueous $NaHCO_3$ (2 × 20 mL) and brine (20 mL), dried over $MgSO_4$, filtered, concentrated in vacuo, and purified by flash chromatography (when specified) to afford the desired compound in excellent yield (85−95%).

*Method B: Preparation of Compounds **3d−k**.* *tert*-Butyl 3,9-diazaspiro[5.5]undecane-3-carboxylate **2** (0.34 mmol, 1 eq) and the appropriate carboxylic acid (1.2 eq) were dissolved in dry CH_2Cl_2 (5 mL). HBTU (1.2 eq), and dry Et_3N (3 eq) were added, and the mixture was stirred at rt overnight. Upon completion, the mixture was diluted with CH_2Cl_2 (30 mL) and washed with saturated aqueous $NaHCO_3$ (3 × 30 mL). The organic layer was dried over Na_2SO_4, filtered, and concentrated in vacuo. Purification by silica gel flash column chromatography provided **3d−k** in very good yields (72−94%).

*Method C: Preparation of Compounds **3l−m** and **3p−q**.* Intermediates **3j−k** and **3n−o** (0.32 mmol, 1.0 eq) were dissolved in dry EtOH (10 mL), and 10% Pd/C (0.1 or 0.6 eq) was added. The reaction mixture was stirred at rt overnight under an H2 atmosphere. After completion, the mixture was filtered through celite, concentrated in vacuo, and purified by flash silica gel chromatography (when specified) to provide **3l−m** and **3p−q** in varying yields (30−100%).

*Method D: Preparation of Compounds **1a−f** and **1j−r**.* In a round-bottomed flask equipped with a magnetic stirring bar, compound **3a−f** or **3j−r** (1.18 mmol, 1.0 eq) was dissolved in dry MeOH (12 mL) unless stated otherwise, and a solution of HCl in dioxane (4N, 2 mL) was added in a dropwise manner. The reaction was stirred for 3 h and then concentrated in vacuo to afford **1a−f** and **1j−r** as hydrochloride salt in very good yields (82−100%).

*Method E: Preparation of Compounds **1g−i**.* Intermediates **3g−i** (0.24 mmol, 1.0 eq) was dissolved in a TFA:CH_2Cl_2 mixture(1:10, 11 mL) and stirred at rt for 3 h. Upon completion, the mixture was cooled to 0 °C and washed with saturated aqueous NaHCO3 (10 mL). The organic layer was dried over MgSO4, filtered, and concentrated in vacuo to afford **1g−i** as white solids in very good yields (80−85%).

*Method F: Preparation of Compounds **4a** and **4b**.* *tert*-Butyl 3,9-diazaspiro[5.5]undecane-3-carboxylate (0.39 mmol, 1.0 eq) and the appropriately substituted benzylbromide (2.0 eq) were dissolved in

https://doi.org/10.1021/acs.jmedchem.1c00290
J. Med. Chem. XXXX, XXX, XXX−XXX

dry CH_2Cl_2 (10 mL). Dry Et3N (2 eq) was added, and the reaction mixture was allowed to stir at rt overnight. Upon completion, the mixture was washed with saturated aqueous NaHCO3 (3 × 20). The organic phase was dried over Na2SO4, filtered, and concentrated in vacuo. Purification by silica gel flash column chromatography (EtOAc:*n*-heptane, 1:1) afforded the desired compounds **4a** or **4b** in good yields (75−98%).

*tert-Butyl 9-Acetyl-3,9-diazaspiro[5.5]undecane-3-carboxylate (**3a**).* Obtained from 305 mg of *tert*-butyl 3,9-diazaspiro[5.5]-undecane-3-carboxylate **2** with acetic anhydride (1.5 eq) and Et_3N (3.0 eq) according to method A. The desired product **3a** was isolated as a transparent oil in 95% yield. R_t (HPLC) = 11.86 min; ^{1}H NMR (600 MHz, $CDCl_3$) δ 3.62−3.49 (m, 2H), 3.49−3.30 (m, 6H), 2.07 (s, 3H), 1.51−1.45 (m, 6H), 1.44 (s, 9H); ^{13}C NMR (151 MHz, $CDCl_3$) δ 169.0, 155.1, 79.6, 42.3, 39.4, 37.3, 36.2, 35.3, 34.7, 30.3, 28.6, 21.6.

*3-(tert-Butyl) 9-Methyl 3,9-Diazaspiro[5.5]undecane-3,9-dicarboxylate (**3b**).* Obtained from 305 mg of *tert*-butyl 3,9-diazaspiro[5.5]undecane-3-carboxylate **2** with methyl chloroformate (1.5 eq) and Et_3N (3.0 eq) according to method A. The desired product **3b** was isolated as a transparent oil in 95% yield. R_t (HPLC) = 13.24 min; ^{1}H NMR (400 MHz, $CDCl_3$) δ 3.66 (s, 3H), 3.46−3.38 (m, 4H), 3.38−3.33 (m, 4H), 1.50−1.38 (m, 17H); ^{13}C NMR (101 MHz, $CDCl_3$) δ 156.1, 155.0, 79.5, 52.6, 39.6, 35.2, 30.1, 28.6.

*tert-Butyl 9-Benzoyl-3,9-diazaspiro[5.5]undecane-3-carboxylate (**3c**).* Obtained from 305 mg of *tert*-butyl 3,9-diazaspiro[5.5]-undecane-3-carboxylate **2** with benzoyl chloride (1.5 eq) and Et_3N (3.0 eq) according to method A. The desired product **3c** was obtained as a white solid in 92% yield after purification by silica gel flash chromatography. R_f (EtOAc:*n*-heptane 1:1) = 0.35; R_t (HPLC) = 13.58 min; ^{1}H NMR (400 MHz, $CDCl_3$) δ 7.41−7.35 (m, 5H), 3.80−3.63 (m, 2H), 3.46−3.28 (m, 6H), 1.50−1.40 (m, 17H); ^{13}C NMR (101 MHz, $CDCl_3$) δ 170.52, 155.05, 136.32, 129.66, 128.58, 126.96, 79.62, 30.55, 28.58, 21.16.

*tert-Butyl 9-(2-Methylbenzoyl)-3,9-diazaspiro[5.5]undecane-3-carboxylate (**3d**).* Obtained from 100 mg of *tert*-butyl 3,9-diazaspiro[5.5]undecane-3-carboxylate **2** with 2-methylbenzoic acid according to method B. The desired product **3d** was obtained as a white solid in 94% yield after purification by silica gel flash chromatography. R_f (EtOAc:*n*-heptane, 1:1) = 0.18; ^{1}H NMR (400 MHz, $CDCl_3$) δ 7.30−7.23 (m, 2H), 7.22−7.16 (m, 2H), 7.16−7.12 (m, 1H), 3.95−3.55 (m, 2H), 3.44−3.29 (m, 4H), 3.28−3.10 (m, 2H), 2.30 (s, 3H), 1.70−1.55 (m, 2H), 1.55−1.41 (m, 13H), 1.41−1.31 (m, 2H). ^{13}C NMR (101 MHz, $CDCl_3$) δ 169.9, 154.9, 136.5, 134.1, 130.4, 128.7, 125.9, 125.6, 79.5, 42.6, 39.2, 37.1, 36.1, 35.5, 35.0, 34.8, 30.4, 28.5, 19.0.

*tert-Butyl 9-(3-Methylbenzoyl)-3,9-diazaspiro[5.5]undecane-3-carboxylate (**3e**).* Obtained from 100 mg of *tert*-butyl 3,9-diazaspiro[5.5]undecane-3-carboxylate **2** with 3-methylbenzoic acid according to method B. The desired product **3e** was obtained as a colorless oil in 79% yield after purification by silica gel flash chromatography. R*f* (EtOAc:*n*-heptane, 1:1) = 0.18; ^{1}H NMR (400 MHz, $CDCl_3$) δ 7.30−7.24 (m, 2H), 7.24−7.18 (m, 2H), 7.16 (d, J = 7.4 Hz, 1H), 3.87−3.55 (m, 2H), 3.39 (t, J = 5.8 Hz, 6H), 2.37 (s, 3H), 1.58 (s, 17H). ^{13}C NMR (101 MHz, $CDCl_3$) δ 170.7, 155.1, 138.5, 136.3, 130.4, 128.4, 127.6, 123.9, 79.6, 35.4, 30.6, 28.6, 21.5.

*tert-Butyl 9-(4-Methylbenzoyl)-3,9-diazaspiro[5.5]undecane-3-carboxylate (**3f**).* Obtained from 100 mg of *tert*-butyl 3,9-diazaspiro[5.5]undecane-3-carboxylate **2** with 4-methylbenzoic acid according to method B. The desired product **3f** was obtained as a colorless oil in 72% yield after purification by silica gel flash chromatography. R*f* (EtOAc:*n*-heptane, 1:1) = 0.18; LC/MS (ESI): m/z calcd for $C_{22}H_{32}N_2O_3$ [M + H]$^+$ = 373.2, found 373.1; ^{1}H NMR (400 MHz, $CDCl_3$) δ 7.29 (d, J = 7.9 Hz, 2H), 7.19 (d, J = 7.9 Hz, 2H), 3.76−3.42 (m, 4H), 3.42−3.35 (m, 4H), 2.37 (s, 3H), 1.45 (s, 17H). ^{13}C NMR (101 MHz, $CDCl_3$) δ 170.6, 154.9, 139.6, 133.2, 129.0, 127.0, 79.5 39.3, 35.2, 30.4, 28.5, 21.4.

*tert-Butyl 9-(2-Bromobenzoyl)-3,9-diazaspiro[5.5]undecane-3-carboxylate (**3g**).* Obtained from 100 mg of *tert*-butyl 3,9-diazaspiro[5.5]undecane-3-carboxylate **2** with 2-bromobenzoic acid according to method B. The desired product **3g** was obtained as a colorless oil in 77% yield after purification by silica gel flash chromatography. R*f* (EtOAc:*n*-heptane, 1:1) = 0.29; LC/MS (ESI): m/z calcd for $C_{21}H_{30}BrN_2O_3$ [M + H]$^+$ = 437.1, 439.1 found 437.0; ^{1}H NMR (400 MHz, $CDCl_3$) δ 7.56 (dd, J = 8.3, 1.2 Hz, 1H), 7.34 (ddd, J = 8.3, 7.3, 1.1 Hz, 1H), 7.25−7.19 (m, 2H), 3.88−3.62 (m, 2H), 3.49−3.29 (m, 4H), 3.24 (ddd, J = 13.8, 8.0, 4.0 Hz, 1H), 3.14 (ddd, J = 13.8, 7.4, 4.0 Hz, 1H), 1.73−1.31 (m, 17H); ^{13}C NMR (101 MHz, $CDCl_3$) δ 167.7, 155.0, 138.5, 132.9, 130.3, 127.8, 127.7, 119.3, 79.6, 42.8, 39.4, 37.4, 35.8, 35.4, 35.0, 34.9, 30.6, 28.6.

*tert-Butyl 9-(3-Bromobenzoyl)-3,9-diazaspiro[5.5]undecane-3-carboxylate (**3h**).* Obtained from 100 mg of *tert*-butyl 3,9-diazaspiro[5.5]undecane-3-carboxylate **2** with 3-bromobenzoic acid according to method B. The desired product **3h** was obtained as a white solid in 82% yield after purification by silica gel flash chromatography. R_f (EtOAc:*n*-heptane, 1:1) = 0.32; LC/MS (ESI): m/z calcd for $C_{21}H_{30}BrN_2O_3$ [M + H]$^+$ = 437.1, 439.1 found 437.0; 1H-NMR (400 MHz, $CDCl_3$) = δ 7.56−7.51 (m, 2H), δ 7.34−7.24 (m, 2H), δ 3.82−3.61 (m, 2H), δ 3.46−3.30 (m, 6H), δ 1.73−1.37 (m, 8H), δ 1.46 (s, 9H); ^{13}C-NMR (101 MHz, $CDCl_3$) δ 168.6, 154.8, 138.1, 132.6, 130.1, 129.3, 125.4, 122.6, 79.5, 39.3, 35.2, 30.4, 28.5.

*tert-Butyl 9-(4-bromobenzoyl)-3,9-diazaspiro[5.5]undecane-3-carboxylate (**3i**).* Obtained from 100 mg of *tert*-butyl 3,9-diazaspiro[5.5]undecane-3-carboxylate **2** with 4-bromobenzoic acid according to method B. The desired product **3i** was obtained as a white solid in 84% yield after purification by silica gel flash chromatography. R_f (EtOAc:*n*-heptane, 1:1) = 0.29; LC/MS (ESI): m/z calcd for $C_{21}H_{30}BrN_2O_3$ [M + H]$^+$ = 437.1, 439.1 found 437.0; ^{1}H NMR (400 MHz, $CDCl_3$) δ 7.54 (d, J = 8.4 Hz, 2H), 7.27 (d, J = 8.4 Hz, 2H), 3.86−3.59 (m, 2H), 3.51−3.28 (m, 6H), 1.73−1.31 (m, 17H); ^{13}C-NMR (101 MHz, $CDCl_3$) δ 169.3, 154.9, 135.0, 131.7, 128.6, 123.8, 79.5, 39.3, 35.1, 30.4, 28.4.

*tert-Butyl 9-(3-(Benzyloxy)benzoyl)-3,9-diazaspiro[5.5]-undecane-3-carboxylate (**3j**).* Obtained from 200 mg of *tert*-butyl 3,9-diazaspiro[5.5]undecane-3-carboxylate **2** with 3-(benzyloxy)-benzoic acid according to method B. The desired product **3j** was obtained as a white solid in 86% yield after purification by silica gel flash chromatography. R*f* (EtOAc:*n*-heptane, 1:1) = 0.29; LC/MS (ESI): m/z calcd for $C_{28}H_{36}N_2O_4$ [M + H]$^+$ = 465.3 found 465.3; ^{1}H NMR (400 MHz, MeOD) δ 7.43 (d, J = 7.1 Hz, 2H), 7.40−7.34 (m, 3H), 7.33−7.27 (m, 1H), 7.16−7.07 (m, 1H), 7.00−6.91 (m, 2H), 5.14 (s, 2H), 3.80−3.60 (m, 2H), 3.48−3.32 (m, 6H), 1.45 (s, 17H). ^{13}C NMR (101 MHz, MeOD) δ 172.0, 160.2, 156.6, 138.5, 138.4, 131.0, 129.58, 129.0, 128.5, 120.1, 117.7, 114.1, 81.0, 71.1, 44.7, 39.1, 36.7, 36.1, 31.6, 28.7.

*tert-Butyl 9-(4-(Benzyloxy)benzoyl)-3,9-diazaspiro[5.5]-undecane-3-carboxylate (**3k**).* Obtained from 200 mg of *tert*-butyl 3,9-diazaspiro[5.5]undecane-3-carboxylate **2** with 4-(benzyloxy)-benzoic acid according to method B. The desired product **3k** was obtained as a white solid in 86% yield after purification by silica gel flash chromatography. R*f* (EtOAc:*n*-heptane, 6:4) = 0.30; LC/MS (ESI): m/z calcd for $C_{28}H_{36}N_2O_4$ [M + H]$^+$ = 465.3 found 465.2; ^{1}H NMR (400 MHz, $CDCl_3$) δ 7.45−7.30 (m, 7H), 6.97 (d, J = 8.7 Hz, 2H), 5.09 (s, 2H), 3.78−3.42 (m, 4H), 3.42−3.35 (m, 4H), 1.58−1.42 (m, 17H). ^{13}C NMR (101 MHz, $CDCl_3$) δ 170.5, 160.0, 155.1, 136.7, 129.1, 128.8, 128.6, 128.2, 127.6, 114.8, 79.6, 70.2, 39.4, 35.4, 35.4, 30.6, 28.6, 22.8, 14.3.

*tert-Butyl 9-(3-Hydroxybenzoyl)-3,9-diazaspiro[5.5]undecane-3-carboxylate (**3l**).* Obtained from 150 mg of **3j** using 10% Pd/C (0.6 eq) in EtOH, according to method C. The desired product **3l** was obtained as a white solid in 76% yield. R_f (EtOAc:*n*-heptane, 1:1) = 0.10; LC/MS (ESI): m/z calcd for $C_{21}H_{30}N_2O_4$ [M + H]$^+$ = 375.5 found 375.5; ^{1}H NMR (400 MHz, MeOD) δ 7.25 (t, J = 7.8 Hz, 1H), 6.90−6.82 (m, 1H), 6.83−6.75 (m, 2H), 3.84−3.68 (m, 2H), 3.51−3.36 (m, 6H), 1.72−1.36 (m, 17H); ^{13}C NMR (101 MHz, MeOD) δ 172.5, 130.9, 118.2, 118.0, 114.6, 81.0, 49.6, 49.4, 49.2, 49.0, 48.8, 48.6, 48.4, 44.8, 39.0, 36.2, 31.6, 28.7.

*tert-Butyl 9-(4-Hydroxybenzoyl)-3,9-diazaspiro[5.5]undecane-3-carboxylate (**3m**).* Obtained from 150 mg of **3k** using 10% Pd/C (0.1

https://doi.org/10.1021/acs.jmedchem.1c00290
J. Med. Chem. XXXX, XXX, XXX−XXX

eq) in EtOH according to method C. The desired product **3m** was obtained as a white solid in 95% yield. R*f* (EtOAc:*n*-heptane, 1:1) = 0.18; LC/MS (ESI): *m/z* calcd for $C_{21}H_{30}N_2O_4$ [M + H]$^+$ = 375.5 found 375.5; ^{1}H NMR (400 MHz, MeOD) δ 7.18 (d, *J* = 8.6 Hz, 2H), 6.73 (d, *J* = 8.6 Hz, 2H), 3.73−3.38 (m, 4H), 3.32 (s, 4H), 1.67−1.21 (m, 17H). ^{13}C NMR (101 MHz, MeOD) δ 172.9, 160.6, 156.6, 130.1, 127.6, 116.2, 81.0, 36.3, 31.6, 28.7.

*tert-Butyl 9-(3-Nitrobenzoyl)-3,9-diazaspiro[5.5]undecane-3-carboxylate (**3n**).* Obtained from 150 mg of *tert*-butyl 3,9-diazaspiro[5.5]undecane-3-carboxylate **2** with 3-nitrobenzoyl chloride (1.2 eq) and Et_3N (2.0 eq) according to method A. The desired product **3n** was obtained as a white solid in 95% yield after purification by silica gel flash chromatography. R*f* (EtOAc:*n*-heptane, 6:4) = 0.29; LC/MS (ESI): *m/z* calcd for $C_{21}H_{30}N_3O_5$ [M + H]$^+$ = 404.2 found 404.1; ^{1}H NMR (400 MHz, MeOD) δ 8.34 (ddd, *J* = 8.2, 2.4, 1.1 Hz, 1H), 8.27 (t, *J* = 1.9 Hz, 1H), 7.81 (dt, *J* = 7.6, 1.3 Hz, 1H), 7.72 (t, *J* = 7.9 Hz, 1H), 3.86−3.69 (m, 2H), 3.50−3.36 (m, 6H), 1.73−1.48 (m, 9H), 1.45 (s, 9H); ^{13}C NMR (101 MHz, MeOD) δ 169.7, 156.6, 149.6, 138.9, 133.9, 131.3, 125.5, 122.9, 81.00, 44.9, 39.3, 36.7, 36.1, 35.8, 31.6, 28.7.

*tert-Butyl 9-(4-Nitrobenzoyl)-3,9-diazaspiro[5.5]undecane-3-carboxylate (**3o**).* Obtained from 145 mg of *tert*-butyl 3,9-diazaspiro[5.5]undecane-3-carboxylate **2** with 4-nitrobenzoyl chloride (1.3 eq) and Et_3N (2.0 eq) according to method A. The desired product **3o** was obtained as a white solid in 95% yield after purification by silica gel flash chromatography. R*f* (EtOAc:*n*-heptane, 6:4) = 0.18; ^{1}H NMR (400 MHz, $CDCl_3$) δ 8.27 (d, *J* = 8.7 Hz, 2H), 7.56 (d, *J* = 8.7 Hz, 2H), 3.92−3.61 (m, 2H), 3.40 (t, *J* = 5.8 Hz, 4H), 3.36−3.23 (m, 2H), 1.74−1.35 (m, 17H). ^{13}C NMR (101 MHz, $CDCl_3$) δ 169.9, 156.9, 150.3, 144.3, 129.8, 125.9, 81.6, 45.5, 41.2, 41.2, 40.0, 38.1, 37.1, 36.7, 32.5, 30.4.

*tert-Butyl 9-(3-Aminobenzoyl)-3,9-diazaspiro[5.5]undecane-3-carboxylate (**3p**).* Obtained from 150 mg of **3n** using 10% Pd/C (0.6 eq) in EtOH according to method C. The desired product **3p** was obtained as a white solid in 76% yield after purification by silica gel flash chromatography. R_f (EtOAc:*n*-heptane, 3:1) = 0.13; LC/MS (ESI): *m/z* calcd for $C_{21}H_{32}N_3O_3$ [M + H]$^+$ = 375.2 found 375.0; ^{1}H NMR (400 MHz, MeOD) δ 7.14 (t, *J* = 7.8 Hz, 1H), 6.76 (ddd, *J* = 8.1, 2.3, 1.0 Hz, 1H), 6.68 (*t*, *J* = 1.9 Hz, 1H), 6.63 (dt, *J* = 7.5, 1.2 Hz, 1H), 3.79−3.63 (m, 2H), 3.51−3.35 (m, 6H), 1.65−1.56 (m, 2H), 1.56−1.47 (m, 6H), 1.45 (s, 9H); ^{13}C NMR (101 MHz, MeOD) δ 173.0, 156.6, 149.6, 137.9, 130.4, 117.4, 116.4, 113.8, 81.0, 44.8, 39.0, 36.9, 36.2, 36.0, 31.6, 28.7.

*tert-Butyl 9-(4-Aminobenzoyl)-3,9-dazaspiro[5.5]undecane-3-carboxylate (**3q**).* Obtained from 70 mg of **3o** using 10% Pd/C (0.1 eq.) in EtOH according to method C. The desired product **3q** was obtained as a white solid in 30% yield after purification by silica gel flash chromatography. R*f* (EtOAc:*n*-heptane, 3:1) = 0.11; LC/MS (ESI): *m/z* calcd for $C_{21}H_{32}N_3O_3$ [M + H]$^+$ = 375.2 found 375.0; ^{1}H NMR (400 MHz, MeOD) δ 7.18 (d, *J* = 8.5 Hz, 2H), 6.69 (d, *J* = 8.5 Hz, 2H), 3.70−3.53 (m, 4H), 3.47−3.35 (m, 4H), 1.60−1.48 (m, 8H), 1.45 (s, 9H); ^{13}C NMR (101 MHz, MeOD) δ 172.03, 155.22, 150.29, 128.59, 123.18, 113.58, 79.54, 34.87, 30.17, 27.29.

*tert-Butyl 9-(4-(Trifluoromethyl)benzoyl)-3,9-diazaspiro[5.5]-undecane-3-carboxylate (**3r**).* Obtained from 305 mg of *tert*-butyl 3,9-diazaspiro[5.5]undecane-3-carboxylate **2** with 4-trifluoromethylbenzoyl chloride (1.5 eq) and Et_3N (3.0 eq) according to method A. The desired product **3r** was obtained as a white solid in 85% yield after purification by silica gel flash chromatography. R_f (EtOAc:*n*-heptane, 1:1) = 0.36; R_t (HPLC) = 14.55 min; ^{1}H NMR (400 MHz, DMSO) δ 7.80 (d, *J* = 8.0 Hz, 2H), 7.59 (d, *J* = 8.0 Hz, 2H), 3.68−3.56 (m, 2H), 3.33−3.26 (m, 4H), 3.22 (m, 2H), 1.38 (m, 17H); ^{13}C NMR (101 MHz, DMSO) δ 167.4, 153.9, 140.5, 127.4, 125.4, 78.4, 42.9, 37.2, 34.9, 34.6, 34.4, 34.3, 30.1, 28.1; ^{19}F NMR (376 MHz, DMSO) δ −61.26.

*1-(3,9-Diazaspiro[5.5]undecan-3-yl)ethan-1-one Hydrochloride (**1a**).* Obtained as a white solid from 349 mg of **3a** according to method D in quantitative yield (100%); R_t (HPLC) = 5.70 min; UPLC/MS (ESI): *m/z* calcd for $C_{11}H_{21}N_2O$ [M + H]$^+$ = 197.2, found 197.2; ^{1}H NMR (400 MHz, DMSO-d_6) δ 9.02 (bs, 2H), 3.44−3.31 (m, 4H), 3.06−2.94 (m, 4H), 1.97 (s, 3H), 1.68−1.59 (m, 4H), 1.45 (t, *J* = 5.8 Hz, 2H), 1.37 (t, *J* = 5.8 Hz, 2H); ^{13}C NMR (101 MHz, DMSO-d_6) δ 168.0, 41.4, 38.8, 36.4, 35.0, 34.1, 31.2, 29.2, 21.3.

*Methyl 3,9-diazaspiro[5.5]undecane-3-carboxylate Hydrochloride (**1b**).* Obtained as a white solid from 435 mg of **3b** according to method D in quantitative yield (100%). R_t (HPLC) = 6.29 min; UPLC/MS (ESI): *m/z* calcd for $C_{11}H_{21}N_2O_2$ [M + H]$^+$ = 213.2, found 213.1; ^{1}H NMR (400 MHz, DMSO-d_6) δ 8.85 (s, 2H), 3.57 (s, 3H), 3.41−3.30 (m, 4H), 3.06−2.96 (m, 4H), 1.61 (t, *J* = 5.9 Hz, 4H), 1.46−1.37 (m, 4H); ^{13}C NMR (101 MHz, DMSO-d_6) δ 155.0, 52.2, 39.0, 38.9, 34.2, 31.2, 28.9.

*Phenyl(3,9-diazaspiro[5.5]undecan-3-yl)methanone Hydrochloride (**1c**).* Obtained as a white solid from 394 mg of **3c** according to method D in quantitative yield (100%). R_t (HPLC) = 7.15 min; UPLC/MS (ESI): *m/z* calcd for $C_{16}H_{23}N_2O$ [M + H]$^+$ = 259.2, found 259.1; ^{1}H NMR (400 MHz, DMSO-d_6) δ 9.01 (s, 2H), 7.47−7.40 (m, 3H), 7.40−7.32 (m, 2H), 3.66−3.52 (m, 2H), 3.37−3.21 (m, 2H), 3.08−2.94 (m, 4H), 1.76−1.62 (m, 4H), 1.57−1.34 (m, 4H); ^{13}C NMR (101 MHz, DMSO-d_6) δ 168.9, 136.4, 129.3, 128.4, 126.6, 40.0, 38.8, 34.1, 31.2, 29.4.

*(2-Methylphenyl)(3,9-diazaspiro[5.5]undecan-3-yl)methanone Hydrochloride (**1d**).* Obtained as a white solid from 111 mg of **3d** according to method D in 97% yield. LC/MS (ESI): *m/z* calcd for $C_{17}H_{25}N_2O$ [M + H]$^+$ = 273.19, found 273.1; ^{1}H NMR (400 MHz, MeOD) δ 7.37−7.23 (m, 3H), 7.19 (dd, *J* = 7.6, 1.5 Hz, 1H), 3.97−3.82 (m, 1H), 3.82−3.62 (m, 1H), 3.28 (t, *J* = 5.8 Hz, 2H), 3.19 (q, *J* = 5.8 Hz, 4H), 2.29 (s, 3H), 1.88−1.74 (m, 4H), 1.73−1.65 (m, 2H), 1.57−1.46 (m, 2H); ^{13}C NMR (101 MHz, MeOD) δ 172.2, 136.9, 135.4, 131.6, 130.4, 127.2, 126.7, 43.9, 41.00, 38.4, 36.4, 35.6, 33.3, 32.3, 30.8, 19.0.

*(3,9-Diazaspiro[5.5]undecan-3-yl)(m-tolyl)methanone Hydrochloride (**1e**).* Obtained as a white solid from 90 mg of **3e** according to method D in 96% yield. R_t (HPLC) = 8.10 min (Figure S7); LC/MS (ESI): *m/z* calcd for $C_{17}H_{25}N_2O$ [M + H]$^+$ = 273.19, found 273.1; ^{1}H NMR (400 MHz, $CDCl_3$) δ 9.47 (bs, 2H), 7.39−6.94 (m, 4H), 3.91−3.21 (m, 4H), 3.22−2.89 (m, 4H), 2.30 (s, 3H), 2.15−1.26 (m, 8H). ^{13}C-NMR (101 MHz, CDCl3) δ 170.7, 138.5, 135.7, 130.6, 128.3, 127.4, 123.8, 39.7, 31.8, 29.8, 21.4.

*(4-Methylphenyl)(3,9-diazaspiro[5.5]undecan-3-yl)methanone Hydrochloride (**1f**).* Obtained as a white solid from 92 mg of **3f** according to method D in quantitative yield. R_t (HPLC) = 8.22 min; LC/MS (ESI): *m/z* calcd for $C_{17}H_{25}N_2O$ [M + H]$^+$ = 273.19, found 273.1; ^{1}H NMR (400 MHz, MeOD) δ 7.39−7.17 (m, 4H), 3.84−3.68 (m, 2H), 3.57−3.38 (m, 2H), 3.25−3.08 (m, 4H), 2.39 (s, 3H), 1.87−1.75 (m, 4H), 1.75−1.48 (m, 4H); ^{13}C NMR (101 MHz, $CDCl_3$) δ 170.9, 140.2, 132.7, 129.3, 127.1, 39.7, 31.9, 29.9, 21.5.

*(2-Bromophenyl)(3,9-diazaspiro[5.5]undecan-3-yl)methanone (**1g**).* Obtained as a white solid from 105 mg of **3 g** according to method E in 80% yield. R_t (HPLC) = 7.91 min; LC/MS (ESI): *m/z* calcd for $C_{16}H_{22}BrN_2O$ [M + H]$^+$ = 337.1, 339.1, found 337.1; ^{1}H NMR (400 MHz, $CDCl_3$) δ 7.70−7.51 (m, 1H), 7.44−7.30 (m, 1H), 7.31−7.13 (m, 2H), 6.04 (bs, 2H), 3.76 (t, *J* = 5.7 Hz, 2H), 3.40−2.91 (m, 5H), 2.45 (t, *J* = 5.7 Hz, 1H), 1.93−1.12 (m, 8H); ^{13}C NMR (101 MHz, $CDCl_3$) δ 167.6, 138.1, 132.9, 130.3, 127.8, 127.5, 119.1, 47.4, 42.8, 42.42, 40.2, 37.4, 37.0, 35.8, 35.6, 35.0, 34.5, 33.2, 33.0, 30.4, 30.0.

*(3-Bromophenyl)(3,9-diazaspiro[5.5]undecan-3-yl)methanone (**1h**).* Obtained as a white solid from 102 mg of **3i** according to method E in 85% yield. R_t (HPLC) = 8.60 min; LC/MS (ESI): *m/z* calcd for $C_{16}H_{22}BrN_2O$ [M + H]$^+$ = 337.1, 339.1, found 337.0; ^{1}H NMR (400 MHz, MeOD) δ 7.69−7.60 (m, 1H), 7.61−7.55 (m, 1H), 7.48−7.30 (m, 2H), 3.85−3.63 (m, 2H), 3.55−3.36 (m, 2H), 3.19 (q, *J* = 5.0 Hz, 4H), 1.79 (t, *J* = 5.5 Hz, 4H), 1.72−1.51 (m, 4H); ^{13}C NMR (101 MHz, MeOD) δ 169.9, 138.6, 133.4, 131.0, 130.1, 125.9, 122.9, 44.0, 40.3, 38.3, 35.6, 34.8, 32.2, 30.1.

*(4-Bromophenyl)(3,9-diazaspiro[5.5]undecan-3-yl)methanone (**1i**).* Obtained as a pale yellow solid from 106 mg of **3i** according to method E in 85% yield. R_t (HPLC) = 8.79 min; LC/MS (ESI): *m/z* calcd for $C_{16}H_{22}BrN_2O$ [M + H]$^+$ = 337.1, 339.1, found 337.0; ^{1}H NMR (400 MHz, $CDCl_3$) δ 7.47 (d, *J* = 8.4 Hz, 2H), 7.20 (d, *J* = 8.4 Hz, 2H), 3.83−3.45 (m, 2H), 3.45−3.17 (m, 2H), 2.83 (t, *J* = 5.7 Hz,

https://doi.org/10.1021/acs.jmedchem.1c00290
J. Med. Chem. XXXX, XXX, XXX−XXX

4H), 2.70 (bs, 2H), 1.85−1.27 (m, 8H); ^{13}C NMR (101 MHz, $CDCl_3$) δ 169.5, 135.0, 131.9, 128.8, 124.1, 41.1, 34.9, 30.4.

*(3-(Benzyloxy)phenyl)(3,9-diazaspiro[5.5]undecan-3-yl)-methanone Hydrochloride (**1j**).* Obtained as a white solid from 47 mg of **3j** according to method D using DCM (5 mL) as solvent in 93% yield. R_t (HPLC) = 10.05 min; LC/MS (ESI): *m/z* calcd for $C_{23}H_{29}N_2O_2$ [M + H]$^+$ = 365.22, found 365.1; ^{1}H NMR (400 MHz, MeOD) δ 7.43 (d, *J* = 7.1 Hz, 2H), 7.41−7.34 (m, 3H), 7.34−7.28 (m, 1H), 7.11 (dd, *J* = 8.3, 2.6 Hz, 1H), 7.00−6.94 (m, 2H), 5.14 (s, 2H), 3.81−3.68 (m, 2H), 3.45−3.33 (m, 2H), 3.19 (q, *J* = 5.4 Hz, 4H), 1.85−1.73 (m, 4H), 1.73−1.57 (m, 2H), 1.57−1.42 (m, 2H); ^{13}C NMR (101 MHz, MeOD) δ 172.1, 160.2, 138.4, 138.3, 131.1, 129.6, 129.0, 128.5, 120.1, 117.7, 114.3, 71.11, 44.53, 40.99, 38.84, 36.36, 32.92, 30.77.

*(4-(Benzyloxy)phenyl)(3,9-diazaspiro[5.5]undecan-3-yl)-methanone Hydrochloride (**1k**).* Obtained as a white solid from 100 mg of **3k** according to method D in quantitative yield. R_t (HPLC) = 9.95 min; LC/MS (ESI): *m/z* calcd for $C_{23}H_{29}N_2O_2$ [M + H]$^+$ = 365.22, found 365.1; ^{1}H NMR (400 MHz, MeOD) δ 7.44 (d, *J* = 6.8 Hz, 2H), 7.41−7.34 (m, 4H), 7.34−7.28 (m, 1H), 7.07 (d, *J* = 8.6 Hz, 2H), 5.14 (s, 2H), 3.82−3.40 (m, 4H), 3.26−3.12 (m, 4H), 1.79 (t, *J* = 5.7 Hz, 4H), 1.72−1.49 (m, 4H); ^{13}C NMR (101 MHz, MeOD) δ 172.5, 161.7, 138.3, 130.0, 129.6, 129.0, 129.0, 128.6, 115.9, 71.1, 41.0, 32.9, 30.8.

*(3-Hydroxyphenyl)(3,9-diazaspiro[5.5]undecan-3-yl)methanone Hydrochloride (**1l**).* Obtained as a white solid from 85 mg of **3l** according to method D in quantitative yield. R_t (HPLC) = 6.46 min; LC/MS (ESI): *m/z* calcd for $C_{16}H_{23}N_2O_2$ [M + H]$^+$ = 275.4, found 275.3; ^{1}H NMR (400 MHz, MeOD) δ 7.16 (t, *J* = 7.9 Hz, 1H), 6.78 (ddd, *J* = 7.9, 2.5, 1.1 Hz, 1H), 6.73 (dt, *J* = 7.9, 1.1 Hz, 1H), 6.71−6.68 (m, 1H), 3.70−3.52 (m, 2H), 3.42−3.27 (m, 2H), 3.15−3.03 (m, 4H), 1.78−1.61 (m, 4H), 1.61−1.50 (m, 2H), 1.47−1.43 (m, 2H). ^{13}C NMR (151 MHz, MeOD) δ 171.0, 157.6, 136.8, 129.5, 117.1, 116.5, 113.1, 43.1, 39.6, 37.4, 35.0, 34.0, 31.5, 29.4.

*(4-Hydroxyphenyl)(3,9-diazaspiro[5.5]undecan-3-yl)methanone Hydrochloride (**1m**).* Obtained as a white solid from 50 mg of **3m** according to method D, in 99% yield. R_t (HPLC) = 6.31 min; LC/MS (ESI): *m/z* calcd for $C_{16}H_{23}N_2O_2$ [M + H]$^+$ = 275.4, found 275.3; ^{1}H NMR (400 MHz, MeOD) δ 7.32 (d, *J* = 8.6 Hz, 2H), 6.86 (d, *J* = 8.6 Hz, 2H), 3.85−3.47 (m, 4H), 3.26−3.12 (m, 4H), 1.85−1.75 (m, 4H), 1.75−1.48 (m, 4H). ^{13}C NMR (101 MHz, MeOD) δ 173.0, 161.1, 130.3, 126.3, 116.3, 49.6, 49.4, 49.2, 49.0, 48.8, 48.6, 48.4, 41.0, 32.9, 30.7.

*(3-Nitrophenyl)(3,9-diazaspiro[5.5]undecan-3-yl)methanone Hydrochloride (**1n**).* Obtained as a white solid from 50 mg of **3n** according to method D using DCM (5 mL) as solvent and stirred at room temperature overnight in quantitative yield. R_t (HPLC) = 7.43 min; LC/MS (ESI): *m/z* calcd for $C_{16}H_{22}N_3O_3$ [M + H] + = 304.4, found 304.3; ^{1}H NMR (400 MHz, MeOD) δ 8.35 (ddd, *J* = 8.3, 2.4, 1.2 Hz, 1H), 8.28 (t, *J* = 1.9 Hz, 1H), 7.83 (dt, *J* = 7.6, 1.4 Hz, 1H), 7.74 (t, *J* = 7.9 Hz, 1H), 3.94−3.68 (m, 2H), 3.56−3.36 (m, 2H), 3.28−3.10 (m, 4H), 1.93−1.76 (m, 4H), 1.76−1.65 (m, 2H), 1.65−1.53 (m, 2H); ^{13}C NMR (101 MHz, MeOD) δ 169.8, 149.6, 138.7, 134.0, 131.3, 125.6, 123.0, 49.6, 49.4, 49.2, 49.0, 48.8, 48.6, 48.4, 44.7, 41.0, 39.1, 35.3, 32.9, 30.8.

*(4-Nitrophenyl)(3,9-diazaspiro[5.5]undecan-3-Yl)methanone Hydrochloride (**1o**).* Obtained as a white solid from 40 mg of **3o** according to method D in quantitative yield. R_t (HPLC) = 7.57 min; LC/MS (ESI): *m/z* calcd for $C_{16}H_{22}N_3O_3$ [M + H]$^+$ = 304.2, found 304.3; ^{1}H NMR (400 MHz, MeOD) δ 8.33 (d, *J* = 8.7 Hz, 2H), 7.66 (d, *J* = 8.7 Hz, 2H), 3.79 (t, *J* = 5.8 Hz, 2H), 3.39 (t, *J* = 5.8 Hz, 2H), 3.27−3.14 (m, 4H), 1.80 (q, *J* = 5.2 Hz, 4H), 1.75−1.65 (m, 2H), 1.64−1.49 (m, 2H). ^{13}C NMR (101 MHz, MeOD) δ 142.6, 128.5, 124.3, 43.9, 40.4, 38.3, 35.7, 35.6, 34.7, 32.3, 30.2.

*(3-Aminophenyl)(3,9-diazaspiro[5.5]undecan-3-yl)methanone Hydrochloride (**1p**).* Obtained as a white solid from 59 mg of **3p** according to method D, using DCM (5 mL) as solvent, in quantitative yield. R_t (HPLC) = 5.01 min; LC/MS (ESI): *m/z* calcd for $C_{16}H_{24}N_3O$ [M + H]$^+$ = 274.2, found 274.2; ^{1}H NMR (400 MHz, MeOD) δ 7.64 (t, *J* = 7.8 Hz, 1H), 7.59−7.48 (m, 2H), 7.46 (t, *J* = 1.9 Hz, 1H), 3.91−3.70 (m, 2H), 3.55−3.37 (m, 2H), 3.28−3.10 (m, 4H), 1.82 (q, *J* = 4.4 Hz, 4H), 1.76−1.49 (m, 4H); ^{13}C NMR (101 MHz, MeOD) δ 170.3, 139.1, 133.0, 131.7, 128.2, 125.4, 122.7, 49.6, 49.4, 49.2, 49.0, 48.8, 48.6, 48.4, 44.7, 41.0, 39.0, 35.4, 32.9, 30.8.

*(4-Aminophenyl)(3,9-diazaspiro[5.5]undecan-3-yl)methanone Hydrochloride (**1q**).* Obtained as a white solid from 19 mg of **3q** according to method D, in 83% yield. R_t (HPLC) = 4.92 min; LC/MS (ESI): *m/z* calcd for $C_{16}H_{24}N_3O$ [M + H]$^+$ = 274.2, found 274.2; ^{1}H NMR (400 MHz, MeOD) δ 7.60 (d, *J* = 8.3 Hz, 2H), 7.52 (d, *J* = 8.3 Hz, 2H), 3.87−3.70 (m, 2H), 3.48−3.37 (m, 2H), 3.27−3.13 (m, 4H), 1.81 (m, 4H), 1.75−1.50 (m, 4H). ^{13}C NMR (101 MHz, MeOD) δ 169.39, 136.38, 132.30, 128.51, 123.12, 43.36, 39.63, 37.64, 31.47, 29.39.

*(3,9-Diazaspiro[5.5]undecan-3-yl)(4-(trifluoromethyl)phenyl)-methanone Hydrochloride (**1r**).* Obtained as a white solid from 435 mg of **3r** according to METHOD D, in 90% yield. R_t (HPLC) = 8.85 min; UPLC/MS (ESI): *m/z* calcd for $C_{17}H_{22}F_3N_2O_2$ [M + H]$^+$ = 327.2, found 327.2; ^{1}H NMR (400 MHz, DMSO-d_6) δ 8.90 (s, 2H), 7.81 (d, *J* = 8.0 Hz, 2H), 7.60 (d, *J* = 8.0 Hz, 2H), 3.67−3.58 (m, 2H), 3.28−3.17 (m, 2H), 3.07−2.93 (m, 4H), 1.73−1.61 (m, 4H), 1.58−1.50 (m, 2H), 1.49−1.38 (m, 2H); ^{13}C NMR (101 MHz, DMSO) δ 167.5, 140.4, 127.4, 125.5, 125.5, 66.3, 31.19, 29.34; ^{19}F NMR (376 MHz, DMSO) δ −61.25.

*tert-Butyl 9-(4-Bromobenzyl)-3,9-diazaspiro[5.5]undecane-3-carboxylate (**4a**).* The compound was obtained from 100 mg of *tert*-butyl 3,9-diazaspiro[5.5]undecane-3-carboxylate and 4-bromobenzylbromide according to method F. Purification by silica gel flash column chromatography (EtOAc:*n*-Heptane, 1:1) yielded **4a** as a light brown solid in 75% yield. R*f* (EtOAc:*n*-Heptane, 1:1) = 0.30; ^{1}H NMR (600 MHz, $CDCl_3$) δ 7.42 (d, *J* = 8.3 Hz, 2H), 7.18 (d, *J* = 8.3 Hz, 2H), 3.44 (s, 2H), 3.40−3.30 (m, 4H), 2.37 (t, *J* = 5.6 Hz, 4H), 1.50 (t, *J* = 5.6 Hz, 4H), 1.44 (s, 9H), 1.41 (t, *J* = 5.7 Hz, 4H). ^{13}C NMR (151 MHz, $CDCl_3$) δ 156.99, 139.55, 133.25, 132.74, 122.71, 81.21, 64.67, 51.00, 41.69, 40.94, 37.38, 31.53, 30.46, 17.26.

*tert-Butyl 9-(3-methylbenzyl)-3,9-diazaspiro[5.5]undecane-3-carboxylate (**4b**).* The compound was obtained from 200 mg of tert-butyl 3,9-diazaspiro[5.5]undecane-3-carboxylate and 3-methylbenzylbromide according to method F. Purification by silica gel flash column chromatography (EtOAc:*n*-heptane, 1:1) yielded **4b** as a colorless oil in 95%. R_f (EtOAc:*n*-heptane, 1:1) = 0.28; LC/MS (ESI): *m/z* calcd for $C_{22}H_{35}N_2O_2$ [M + H]$^+$ = 359.5, found 359.3; ^{1}H NMR (600 MHz, $CDCl_3$) δ 7.20 (t, J = 7.5 Hz, 1H), 7.16−7.12 (m, 1H), 7.12−7.08 (m, 1H), 7.08−7.05 (m, 1H), 3.47 (s, 2H), 3.41−3.28 (m, 4H), 2.51−2.35 (m, 4H), 2.34 (s, 3H), 1.56−1.48 (m, 4H), 1.45 (s, 9H), 1.44−1.34 (m, 4H). 13C-NMR (151 MHz, $CDCl_3$) δ 157.0, 139.8, 133.8, 132.0, 130.1, 129.8, 128.4, 81.2, 65.4, 51.0, 37.3, 31.5, 30.5, 23.4.

*3-(4-Bromobenzyl)-3,9-diazaspiro[5.5]undecane TFA (**1s**).* Obtained as a white solid from 101 mg of **4a** according to method E in 19% yield after purification by preparative HPLC. R_t (HPLC) = 6.89 min; LC/MS (ESI): *m/z* calcd for $C_{16}H_{24}BrN_2$ [M + H]$^+$ = 323.1, 325.1 found 323.0, 325.0; ^{1}H NMR (400 MHz, MeOD) δ 7.66 (d, *J* = 8.4 Hz, 2H), 7.43 (d, *J* = 8.4 Hz, 2H), 4.32 (s, 2H), 3.42−3.33 (m, 2H), 3.25−3.06 (m, 6H), 2.08−1.85 (m, 4H), 1.79−1.59 (m, 4H). ^{13}C NMR (101 MHz, MeOD) δ 161.6, 134.2, 133.6, 129.8, 129.5, 125.6, 121.2, 74.7, 60.5, 48.0, 40.8, 36.2, 32.9, 29.4, 28.5.

*3-(3-Methylbenzyl)-3,9-diazaspiro[5.5]undecane Hydrochloride (**1t**).* Obtained as a white solid from 222 mg of **4b** according to method D using dry CH_2Cl_2 (10 mL) as a solvent in 95% yield. R_t (HPLC) = 6.13 min; LC/MS (ESI): *m/z* calcd for $C_{17}H_{27}N_2$ [M + H]$^+$ = 259.4 found 259.3; ^{1}H NMR (400 MHz, MeOD) δ 7.43−7.38 (m, 1H), 7.38−7.29 (m, 3H), 4.32 (s, 2H), 3.35 (dt, *J* = 12.5, 2.6 Hz, 2H), 3.28−3.10 (m, 6H), 2.39 (s, 3H), 2.11−1.90 (m, 4H), 1.83−1.67 (m, 4H); ^{13}C NMR (101 MHz, MeOD) δ 140.5, 132.9, 131.9, 130.3, 130.2, 129.4, 61.4, 41.0, 40.8, 36.1, 32.9, 29.5, 28.5, 21.3.

*2-(Chloromethyl)thiophene (**6**).* In a Schlenk dry round-bottomed flask equipped with a magnetic stirring bar and under a N_2 atmosphere, to a solution of thien-2-ylmethanol **5** (5.00 g, 43.8 mmol, 4.17 mL, 1 eq) in dry CH_2Cl_2 (50 mL) was added $SOCl_2$ (10.42 g, 87.6 mmol, 6.36 mL, 2 eq) in a dropwise manner. The

https://doi.org/10.1021/acs.jmedchem.1c00290
J. Med. Chem. XXXX, XXX, XXX−XXX

solution was left at room temperature for 4 h, quenched with saturated $NaHCO_3$ (20 mL) and extracted with CH_2Cl_2 (2 × 30 mL), dried over $MgSO_4$, filtered, and concentrated in vacuo to afford **6** in quantitative yield (5.81 g, 100%). ^{1}H NMR (600 MHz, $CDCl_3$) δ 7.33 (dd, J = 5.1, 1.2 Hz, 1H), 7.10 (dd, J = 3.5, 1.2 Hz, 1H), 6.98 (dd, J = 5.1, 3.5 Hz, 1H), 4.83 (s, 2H); ^{13}C NMR (151 MHz, $CDCl_3$) δ 140.20, 127.78, 127.01, 126.99, 40.47.

*Methyl 3-(Thiophen-2-ylmethoxy)benzoate (**7**).* In a Schlenk dry round-bottomed flask equipped with a magnetic stirring bar and under a N_2 atmosphere, methyl-3-hydroxy benzoate (456.6 mg, 3.00 mmol, 1 eq) and K_2CO_3 (829.3 mg, 6.00 mmol, 2 eq) were suspended in dry DMF (30 mL) followed by addition of **6** (437.6 mg, 3.30 mmol, 1.1 eq). The reaction was heated to 75 °C and left for 2 h, quenched with H_2O (30 mL), and transferred to a separatory funnel and extracted with EtOAc (2 × 50 mL). The combined organic layer was washed with H_2O (5 × 30 mL) and brine (30 mL), dried over $MgSO_4$, filtered, and concentrated in vacuo to afford **7** as a brown liquid (750 mg, 100%). ^{1}H NMR (400 MHz, $CDCl_3$) δ 7.59−7.53 (m, 2H), 7.27−7.20 (m, 2H), 7.06 (dd, J = 8.3, 2.7 Hz, 1H), 7.02 (dd, J = 3.5, 1.0 Hz, 1H), 6.90 (dd, J = 5.1, 3.5 Hz, 1H), 5.15 (s, 2H), 3.80 (s, 3H). ^{13}C NMR (101 MHz, $CDCl_3$) δ 166.9, 158.3, 138.9, 131.6, 129.6, 127.13, 126.9, 126.5, 122.6, 120.5, 115.3, 65.2, 52.3.

*3-(Thiophen-2-ylmethoxy)benzoic Acid (**8**).* Compound **7** (750 mg, 3.00 mmol, 1 eq) was dissolved in a mixture of H_2O and THF (1:2, 15 mL) followed by addition of NaOH (298.5 mg, 6.00 mmol, 2 eq) and stirred overnight. The reaction mixture was transferred with aqueous HCl (4 N, 20 mL) and extracted with EtOAc (3 × 20 mL). The combined organic layer was dried over $MgSO_4$, filtered, and concentrated in vacuo to afford **7** as a white solid (619.4 mg, 88.1%). ^{1}H NMR (600 MHz, $CDCl_3$) δ 7.75 (dt, J = 7.9, 1.1 Hz, 1H), 7.73 (dd, J = 2.7, 1.1 Hz, 1H), 7.40 (t, J = 7.9 Hz, 1H), 7.35 (dd, J = 5.1, 1.1 Hz, 1H), 7.24 (ddd, J = 7.9, 2.7, 1.1 Hz, 1H), 7.14 (dd, J = 3.5, 1.1 Hz, 1H), 7.02 (dd, J = 5.1, 3.5 Hz, 1H), 5.29 (s, 2H); ^{13}C NMR (151 MHz, $CDCl_3$) δ 171.8, 158.4, 138.8, 130.7, 129.8, 127.3, 127.0, 126.6, 123.4, 121.6, 115.7, 65.3.

*tert-Butyl 9-(2,2,2-Trifluoroacetyl)-3,9-diazaspiro[5.5]undecane-3-carboxylate (**9**).* In a Schlenk flame-dried round-bottomed flask equipped with a magnetic stirring bar, *tert*-butyl 3,9-diazaspiro[5.5]-undecane-3-carboxylate **2** (2.0 g, 7.86 mmol, 1 eq) and dry Et_3N (2.39 g, 23.59 mmol, 3.29 mL, 3 eq) were dissolved in dry CH_2Cl_2 (40 mL) under a N_2 atmosphere. The reaction mixture was cooled to 0 °C in an ice water bath following dropwise addition of trifluoroacetic anhydride (2.48 g, 11.79 mmol, 1.64 mL, 1.5. eq). The reaction mixture was left overnight. After quenching with saturated aqueous $NaHCO_3$ (40 mL), the aqueous layer was extracted with CH_2Cl_2 (3 × 30 mL). The combined organic layer was washed with saturated aqueous $NaHCO_3$ (30 mL) and brine (30 mL), dried over $MgSO_4$, filtered, and concentrated in vacuo to afford **9** as a white crystalline solid (2.73 g, >95%); ^{1}H NMR (400 MHz, $CDCl_3$) δ 3.63 (m, 2H), 3.54 (t, J = 5.8 Hz, 2H), 3.39 (t, J = 5.9 Hz, 4H), 1.56 (t, J = 5.9 Hz, 4H), 1.49 (t, J = 5.8 Hz, 4H), 1.45 (s, 9H); ^{13}C NMR (101 MHz, $CDCl_3$) δ 155.4, 155.0, 118.1, 79.7, 46.2, 41.7, 41.6, 39.4, 35.9, 34.7, 30.4, 28.6; ^{19}F NMR (376 MHz, $CDCl_3$) δ −68.93.

*2,2,2-Trifluoro-1-(3,9-diazaspiro[5.5]undecan-3-yl)ethan-1-one (**10**).* In a round-bottomed flask equipped with a magnetic stirring bar, compound **9** (2.73 g, 7.86 mmol, 1.0 eq) was dissolved in dry MeOH (50 mL), and a solution of HCl in dioxane (4N, 10 mL) was added dropwise. The reaction was left for 2 h before concentration in vacuo to afford **10** as a hydrochloride salt in quantitative yield (2.26 g, >95%); UPLC/MS (ESI): m/z calcd for $C_{11}H_{18}F_3N_2O$ $[M + H]^+$ = 251.3, found 251.1; ^{1}H NMR (400 MHz, MeOD) δ 3.72−3.60 (m, 4H), 3.26−3.16 (m, 4H), 1.89−1.75 (m, 4H), 1.72−1.58 (m, 4H); ^{13}C NMR (101 MHz, MeOD) δ 157.00, 156.65, 156.29, 155.94 (quartet splitting from F), 122.33, 119.48, 116.62, 113.77 (quartet splitting from F), 47.89, 42.60, 42.57, 40.93, 40.80, 40.23, 36.26, 35.21, 32.70, 32.52, 30.65, 9.22.; ^{19}F NMR (376 MHz, MeOD) δ −70.45.

*2,2,2-Trifluoro-1-(9-(3-(thiophen-2-ylmethoxy)benzoyl)-3,9-diazaspiro[5.5]undecan-3-yl)ethan-1-one (**3u**).* In a round-bottomed flask equipped with a magnetic stirring bar, **8** (337.03 mg, 1.44 mmol, 1.2 eq) and compound **10** (300 mg, 1.20 mmol, 1 eq) were dissolved in dry CH_2Cl_2 (25 mL), followed by the addition of HBTU (545.5 mg, 1.44 mmol, 1.2 eq) and dry Et_3N (363.9 mg, 0.50 mL, 3 eq). The reaction was stirred at rt overnight, diluted with CH_2Cl_2 (25 mL), and washed with saturated $NaHCO_3$ (3 × 50 mL). The organic layer was then dried over $MgSO_4$, filtered, and concentrated in vacuo. The crude brown oil was purified by silica gel flash column chromatography using a gradient (EtOAc:*n*-heptane 1:1 to EtOAc) to afford **3u** as a viscous oil (403.6 mg, 73%). R_f = 0.15 (EtOAc:*n*-heptane 1:1); UPLC/MS (ESI): m/z calcd for $C_{23}H_{25}F_3N_2O_3S$ $[M + H]^+$ = 467.2, found 467.2; ^{1}H NMR (400 MHz, DMSO) δ 7.55 (dd, J = 5.1, 1.2 Hz, 1H), 7.35 (dd, J = 8.2, 7.5 Hz, 1H), 7.21 (dd, J = 3.5, 1.2 Hz, 1H), 7.08 (ddd, J = 8.2, 2.7, 1.1 Hz, 1H), 7.04 (dd, J = 5.1, 3.5 Hz, 1H), 6.99 (dd, J = 2.7, 1.3 Hz, 1H), 6.94 (dt, J = 7.5, 1.3 Hz, 1H), 5.32 (s, 2H), 3.68−3.43 (m, 6H), 3.29−3.18 (m, 2H), 1.67−1.38 (m, 8H); ^{13}C NMR (101 MHz, DMSO) δ 168.41, 157.64, 138.99, 137.79, 129.65, 127.56, 126.83, 119.08, 115.98, 112.94, 64.33, 38.97, 35.00, 33.98, 30.43, 22.07, 14.05; ^{19}F NMR (376 MHz, DMSO) δ −68.07.

*(3,9-Diazaspiro[5.5]undecan-3-yl)(3-(thiophen-2-ylmethoxy)-phenyl)methanone (**1u**).* In a round-bottomed flask equipped with a magnetic stirring bar, compound **3u** (403.6 mg, 0.87 mmol, 1 eq) was dissolved in a solvent mixture consisting of EtOH (5 mL) and 10% aqueous NaOH (2.5 mL). The reaction was left for 2 h before being diluted with H_2O (25 mL) and extracted with CH_2Cl_2 (3 × 25 mL). The combined organic layers were dried over $MgSO_4$, filtered, and concentrated in vacuo to afford **1u** as a viscous oil (250.3 mg, 78.0%); R_t (HPLC) = 14.22 min; UPLC/MS (ESI): m/z calcd for $C_{21}H_{27}N_2O_2S$ $[M + H]^+$ = 371.2, found 371.2; ^{1}H NMR (400 MHz, DMSO) δ 7.55 (dd, J = 5.1, 1.2 Hz, 1H), 7.34 (t, J = 7.9 Hz, 1H), 7.21 (dd, J = 3.5, 1.2 Hz, 1H), 7.07 (ddd, J = 7.9, 2.6, 1.2 Hz, 1H), 7.03 (dd, J = 5.1, 3.5 Hz, 1H), 6.97 (dd, J = 2.6, 1.2 Hz, 1H), 6.92 (dt, J = 7.9, 1.2 Hz, 1H), 5.32 (s, 2H), 3.67−3.49 (m, 2H), 3.33−3.12 (m, 4H), 2.68−2.59 (m, 2H), 1.50−1.32 (m, 8H); ^{13}C NMR (101 MHz, DMSO) δ 205.99, 195.26, 176.65, 175.53, 167.27, 165.19, 164.47, 164.45, 156.72, 153.57, 150.54, 101.96, 78.74, 75.86, 73.49, 67.88.

[^{3}H]-Muscimol Binding Assay. The [^{3}H]-muscimol binding assays were performed using cortical synaptic membranes prepared as previously described.[26] On the day of the experiment, the membrane preparation was quickly thawed, homogenized in 40 volumes of 50 mM Tris−HCl buffer (pH 7.4), and centrifuged at 20,000 rpm for 10 min at 4 °C. The washing step was repeated four consecutive times. The final pellet was resuspended in buffer.

Incubation of membranes in 96-well plates (70−80 μg protein) in 200 μL of buffer, 25 μL of [^{3}H]-muscimol (5 nM final concentration), and 25 μL of test compounds in various concentrations for at 0 °C. The reaction was terminated by rapid filtration through Whatman GF/C filters (PerkinElmer Life Sciences) using a 96-well Packard FilterMate cell-harvester followed by washing with 3 × 250 μL of ice-cold buffer. Upon drying the filters overnight at 50 °C, 30 μL of Microscint scintillation fluid (PerkinElmer Life Sciences) was added, and the amount of filter-bound radioactivity was quantified in cpm. The experiments were performed in triplicate at least three times per compound. Nonspecific binding was determined using 1.0 mM GABA and total binding was determined using buffer solution. The binding data were analyzed by a nonlinear regression curve-fitting procedure using GraphPad Prism 7.02 (GraphPad Software Inc., San Diego, CA, USA).

FLIPR Membrane Potential Assay. Cell line origin has been previously described in detail.[26,53] A HEK293 Flp-In cell line stably expressing the human δ-GABA$_A$ receptor subunit (δ-HEK), a HEK293 Flp-In background cell line stably expressing the G-protein-coupled receptor NPBWR2, and the HEK293 cell line stably expressing the human $\alpha_1\beta_2\gamma_2$ receptors were maintained in DMEM containing GlutaMAX-I supplemented with 10% fetal bovine serum (FBS) and 1% penicillin−streptomycin and kept in an incubator at 37 °C with a humidity of 5% CO_2. HEK Flp-In cell lines were positively selected using 200 μg/mL hygromycin B. All cell media and additives were from Life Technologies (Paisley, UK).

https://doi.org/10.1021/acs.jmedchem.1c00290
J. Med. Chem. XXXX, XXX, XXX−XXX

Transfection of δ-HEK cells and HEK background cells was attained using half amounts of Polyfect transfection reagent (Qiagen, West Sussex, UK) with α and β-subunits in a 1:1 ratio or α, β, and γ in a 1:1:2 ratio to express $\alpha\beta\delta$ or $\alpha\beta\gamma$ receptors, respectively. The cells were transfected with human $GABA_A$ receptor subunits α_1, α_2, α_3, α_5, α_6, β_2, γ_2 (pcDNA3.1/Zeo), α_4, and β_1 (pUNIV) to obtain the respective subtypes.

The FMP assay was performed as described previously.[26] GABA EC_{80} concentrations applied to test the antagonist activities of the compounds were determined from full GABA concentration−response curves at the respective receptor subtypes. The obtained relative changes in fluorescence units (ΔRFU) are the difference between the baseline fluorescent signal measured before compound addition and the peak/top plateau in the fluorescent signal obtained after buffer/compound addition. Signal artifacts due to compound/buffer addition was removed from the data based on manual inspection of the raw data traces. Concentration−inhibition curves used to determine antagonist potency were fitted using the four-parameter concentration−response model:

$$\text{response} = \text{bottom} + \frac{\text{top} - \text{bottom}}{1 + 10^{[(\log IC_{50} - A)\cdot n_H]}}$$

where IC_{50} is the concentration of the compound A resulting in the half-maxium response (reponse halftway between top and bottom) and n_H is the Hill coefficient. Data analysis was performed using GraphPad Prism v.8 (GraphPad Software Inc., San Diego, CA, USA).

Whole-Cell Patch-Clamp Electrophysiology. Whole-cell patch-clamp experiments were performed essentially as described previously[26] with the following modifications.

δ-HEK cells transiently expressing human $\alpha_4\beta_1\delta$ or $\alpha_1\beta_2\delta$ receptors were seeded in 35 mm Petri dishes 1 day after transfection and 1−2 days before the experiments. Initially, in GABA concentration−response experiments, for each receptor, a GABA concentration (EC_{90-100}) eliciting a close to maximum peak response was established in order to ensure fast activation of the receptors. GABA concentrations of 100 μM and 1 mM for the $\alpha_4\beta_1\delta$ and $\alpha_1\beta_2\delta$ receptors, respectively, were found to be suitable.

For the kinetic studies, various concentrations of **1e** were applied for 20 s, immediately followed by application of GABA (EC_{90-100}) alone for 5 s or until a peak or plateau current response was reached. The cells were allowed to recover so that GABA applications were at least 1 min apart.

The preapplication of **1e** concentration-dependently protracted the subsequent receptor activation by GABA. In order to describe this effect, the activation phase was fitted with two exponential components (biexponantial fitting), where applicable, or otherwise with one exponential component using a Simplex optimization algorithm (PulseFit; HEKA, Germany).[26] This procedure lead to two (τ_{fast}, τ_{slow}) or one (τ) time constants, respectively. When biexponential fitting was applied, the fractional amplitude of the fast component $\%A_{fast} = (A_{fast}/(A_{slow} + A_{fast}))$ was also calculated. For comparison with τ values from monoexponantial fitting, a weighted time constant (τ_w) was calculated.

$$\tau_w = \frac{\tau_{fast}\cdot\%A_{fast} + \tau_{slow}\cdot(1 - \%A_{fast})}{100\%}$$

τ values are reported as medians with interquartile (25−75%) intervals and compared using Kruskal−Wallis ANOVA followed by Dunn's multiple comparison.

In order to estimate the concentration resulting in 50% receptor occupation by **1e**, corresponding to a "functional" K_B, the following concentration−inhibition model was fitted to the concentration−% A_{fast} data (GraphPad Prism v.7, GraphPad Software Inc., San Diego, CA, USA).

$$\%A_{fast} = \frac{100\%}{1 + 10^{[(\log IC_{50} - [\mathbf{1e}])\cdot n_H]}}$$

Membrane Permeability. Bidirectional permeability was tested for **1e** in the Madin−Darby canine kidney (MDCK) cell line expressing human multidrug resistance protein (MDR1, *P*-glycoprotein) (referred to as MDR1-MDCK cells) as described previously.[54] To calculate efflux ratio, the permeability in the basal-to-apical direction was divided by the permeability in the apical-to-basal direction. The obtained data is from triplicate measurements.

Molecular Modeling. *Ligand Preparation.* Compounds **2027**, **018**, and **1a−u** were prepared with the 2D sketch editor of Maestro, and their protonation state was assigned with Ligprep using default settings.[55]

Receptor Preparation and Docking. The extracellular β_3/α_1 interface, complexed with bicuculline (BCC), was extracted from the cryo-EM of $\alpha_1\beta_3\gamma_{2L}$ $GABA_AR$ (PDB code: 6HUK)[32] and prepared with the Protein Preparation Wizard with default settings.[56] Then, the shape and size of the binding pocket was adapted to the shape and size of our ligands by docking the compound with the highest binding affinity in the [^{3}H]-muscimol assay (**018**) using the Induced Fit Docking Protocol.[57] The docking center was defined by the complexed BCC, a scaling factor of 0.8 was used to avoid excessive deformation of the binding site, and default settings were used elsewhere. Compounds **2027**, **018**, and **1a−u** were then docked using Glide XP Ligand Docking Protocol with default settings on a grid centered on the present ligand.[58] The best scoring output pose according to the XP GScore was selected for each ligand. In all cases, the selected pose also maintained the conserved electrostatic interaction between the ammonium group and Glu 155. The inner surface of the receptor was calculated with SiteMap.[59]

T Cell Proliferation Assay. *PBMC Isolation.* Anonymized leukocyte cones were obtained with consent from the National Blood Service (Southampton, UK) and were used within 4 h for preparation of peripheral blood mononuclear cells (PBMC) by density gradient centrifugation (Lymphoprep; Stemcell Technologies, Cambridge, UK). Residual red blood cells were removed through the addition of ammonium−chloride−potassium lysing buffer (Thermo-Fisher Scientific, Massachusetts, USA), and contaminating platelets were eliminated by three slow-speed centrifugations (200*g*, 10 min), in Roswell Park Memorial Institute (RPMI) 1640 medium (Sigma-Aldrich, Dorset, UK). Finally, PBMCs were resuspended in freezing medium (composed of 90% (v/v) fetal calf serum (FCS) and 10% (v/v) DMSO (Sigma-Aldrich)), initially frozen at −80 °C, and then subsequently transferred to liquid nitrogen for extended storage.

Splenocyte Isolation. Spleens were harvested from female wild-type BALB/c mice. Splenocytes were isolated through processing the spleen into a single-cell suspension using a cell strainer and subsequent collection of the cells in phosphate buffered saline (PBS). Residual red blood cells were removed through the addition of ammonium−chloride−potassium lysing buffer before the remaining splenocytes were resuspended in RPMI 1640 medium containing 10% FCS, L-glutamine, pyruvate, antibiotics penicillin and streptomycin, and 2 μM 2-betamercaptoethanol (Sigma-Aldrich).

Proliferation Assay Experimental Setup. PBMC and splenocytes were isolated as described above and resuspended in PBS at a density of 1×10^7 cells/ml. Cells were then stained with 5 μM CFSE (BioLegend, San Diego, USA) and incubated at room temperature for 10 min protected from light. RPMI medium containing 10% FCS, L-glutamine, pyruvate, and antibiotics penicillin and streptomycin was added to cells to quench the CFSE, and the cells were centrifuged for 5 min at 300*g* before being resuspended in RPMI medium containing 10% FCS, L-glutamine, pyruvate, and antibiotics penicillin and streptomycin. PBMCs were subjected to high-density incubation overnight (at a concentration of 1×10^7 cells/ml) prior to commencement of the proliferation assay as previously described.[60]

Cells were activated with soluble anti-CD3 antibody (anti-human CD3: clone OKT3 and anti-mouse CD3: clone 145.2C11, both made in-house, and < 10 EU/mg endotoxin) at concentrations indicated in the individual figure legends. In addition, alprazolam, BMI (both from Sigma-Aldrich), and **1e** were used as activating or inhibitory reagents within the assay. The concentrations of each reagent used within individual experiments are indicated in the individual figure legends.

PBMC were incubated for 96 h, while splenocytes were incubated for 48 h. Cells were then harvested, and the percentage of

https://doi.org/10.1021/acs.jmedchem.1c00290
J. Med. Chem. XXXX, XXX, XXX−XXX

proliferating cells in each condition were determined through flow cytometry as described below.

Flow Cytometry. The following antibodies were used for flow cytometry: mouse anti-human APC-CD8(SK1), mouse anti-human PE-CD4(OKT4), rat anti-mouse PE-CD4(GK1.5), and rat anti-mouse APC-CD8(53−6.7), in addition to the appropriate isotype controls (all from BioLegend). Cells were harvested and washed in flow cytometry buffer (PBS supplemented with 1% (w/v) BSA, 0.1% (w/v) sodium azide, and 0.5 mM EDTA (all from Sigma-Aldrich)) before being stained with fluorochrome-conjugated antibodies according to the manufacturer's instructions. Following staining, cells were washed three times in flow cytometry buffer before being fixed with 1% (w/v) paraformaldehyde (BD Biosciences, Oxford, UK).

Flow cytometry was performed on a FACSCalibur using BD Cellquest software or on a FACSCanto-II using BD FACSDiva software. Further analysis and figure preparation were carried out using FlowJo software.

■ ASSOCIATED CONTENT

Supporting Information

The Supporting Information is available free of charge at https://pubs.acs.org/doi/10.1021/acs.jmedchem.1c00290.

Molecular formula string (CSV)

Supplementary docking information (PDB)

Supplementary figures (PDF)

■ AUTHOR INFORMATION

Corresponding Author

Bente Frølund − *Department of Drug Design and Pharmacology, Faculty of Health and Medical Sciences, University of Copenhagen, DK-2100 Copenhagen, Denmark;* orcid.org/0000-0001-5476-6288; Phone: +45 35336495; Email: bfr@sund.ku.dk

Authors

Francesco Bavo − *Department of Drug Design and Pharmacology, Faculty of Health and Medical Sciences, University of Copenhagen, DK-2100 Copenhagen, Denmark*

Heleen de-Jong − *Department of Drug Design and Pharmacology, Faculty of Health and Medical Sciences, University of Copenhagen, DK-2100 Copenhagen, Denmark*

Jonas Petersen − *Department of Drug Design and Pharmacology, Faculty of Health and Medical Sciences, University of Copenhagen, DK-2100 Copenhagen, Denmark; Novo Nordisk Foundation Center for Basic Metabolic Research, Faculty of Health and Medical Sciences, University of Copenhagen, DK-2200 Copenhagen, Denmark*

Christina Birkedahl Falk-Petersen − *Department of Drug Design and Pharmacology, Faculty of Health and Medical Sciences, University of Copenhagen, DK-2100 Copenhagen, Denmark*

Rebekka Löffler − *Department of Drug Design and Pharmacology, Faculty of Health and Medical Sciences, University of Copenhagen, DK-2100 Copenhagen, Denmark*

Emma Sparrow − *Antibody and Vaccine Group, Centre for Cancer Immunology, MP127, University of Southampton Faculty of Medicine, Southampton SO16 6YD, United Kingdom*

Frederik Rostrup − *Department of Drug Design and Pharmacology, Faculty of Health and Medical Sciences, University of Copenhagen, DK-2100 Copenhagen, Denmark*

Jannik Nicklas Eliasen − *Department of Drug Design and Pharmacology, Faculty of Health and Medical Sciences, University of Copenhagen, DK-2100 Copenhagen, Denmark*

Kristine S. Wilhelmsen − *Department of Drug Design and Pharmacology, Faculty of Health and Medical Sciences, University of Copenhagen, DK-2100 Copenhagen, Denmark*

Kasper Barslund − *Translational DMPK, 2500 Valby, Denmark*

Christoffer Bundgaard − *Translational DMPK, 2500 Valby, Denmark*

Birgitte Nielsen − *Department of Drug Design and Pharmacology, Faculty of Health and Medical Sciences, University of Copenhagen, DK-2100 Copenhagen, Denmark*

Uffe Kristiansen − *Department of Drug Design and Pharmacology, Faculty of Health and Medical Sciences, University of Copenhagen, DK-2100 Copenhagen, Denmark*

Petrine Wellendorph − *Department of Drug Design and Pharmacology, Faculty of Health and Medical Sciences, University of Copenhagen, DK-2100 Copenhagen, Denmark;* orcid.org/0000-0002-5455-8013

Yury Bogdanov − *Antibody and Vaccine Group, Centre for Cancer Immunology, MP127, University of Southampton Faculty of Medicine, Southampton SO16 6YD, United Kingdom*

Complete contact information is available at: https://pubs.acs.org/10.1021/acs.jmedchem.1c00290

Author Contributions

The manuscript was written through contributions of all authors. F.B. performed the modeling studies and wrote the first draft of the manuscript. H.J. and J.P. synthesized the compounds. C.F.P., R.L., and P.W. performed FMP assays. B.N. and H.J. performed radioligand binding assay. J.N.E. and U.K. performed electrophysiology. E.S. and Y.B. performed T cell proliferation assays. F.R. performed some preliminary docking studies. B.F. devised the study, supervised the work, and revised the manuscript. All authors have given approval to the final version of the manuscript.

Notes

The authors declare no competing financial interest.

■ ACKNOWLEDGMENTS

This work was supported by the Lundbeck Foundation (R303-2018-3346). Y.B. and E.L.S. were supported by the Cancer Research UK Pioneer Award to Y.B. (C55651/A26704).

■ ABBREVIATIONS

ANOVA, analysis of variance; BBFO, broadband fluorine observation; BCC, bicuculline; BMI, bicuculline methiodide; CD, cluster of differentiation; CFSE, carboxyfluorescein succinimidyl ester; cryo-EM, cryogenic electron microscopy; DAD, diode array detection; FACS, fluorescence-assisted cell sorting; FCS, fetal calf serum; FMP, FLIPR membrane potential; H2BC, heteronuclear 2-bond correlation; HBTU, hexafluorophosphate benzotriazole tetramethyl uronium; PAM, positive allosteric modulator; PDA, photodiode array; PMBC, peripheral blood mononuclear cells; RPMI, Roswell Park Memorial Institute; SEM, standard error of the mean; TOCSY, total correlation spectroscopy

REFERENCES

(1) Whiting, P. J. GABA-A receptor subtypes in the brain: a paradigm for CNS drug discovery? *Drug Discovery Today* **2003**, *8*, 445−450.

(2) Fritzius, T.; Bettler, B. The organizing principle of $GABA_B$ receptor complexes: physiological and pharmacological implications. *Basic Clin. Pharmacol. Toxicol.* **2020**, *126*, 25−34.

(3) Olsen, R. W.; Sieghart, W. International union of pharmacology. LXX. Subtypes of γ-aminobutyric $acid_A$ receptors: classification on the basis of subunit composition, pharmacology, and function. Update. *Pharmacol. Rev.* **2008**, *60*, 243−260.

(4) Foster, A. C.; Kemp, J. A. Glutamate- and GABA-based CNS therapeutics. *Curr. Opin. Pharmacol.* **2006**, *6*, 7−17.

(5) Everington, E. A.; Gibbard, A. G.; Swinny, J. D.; Seifi, M. Molecular characterization of GABA-A receptor subunit diversity within major peripheral organs and their plasticity in response to early life psychosocial stress. *Front. Mol. Neurosci.* **2018**, *11*, 18.

(6) Januzi, L.; Poirier, J. W.; Maksoud, M. J. E.; Xiang, Y. Y.; Veldhuizen, R. A. W.; Gill, S. E.; Cregan, S. P.; Zhang, H.; Dekaban, G. A.; Lu, W. Y. Autocrine GABA signaling distinctively regulates phenotypic activation of mouse pulmonary macrophages. *Cell. Immunol.* **2018**, *332*, 7−23.

(7) Bhat, R.; Axtell, R.; Mitra, A.; Miranda, M.; Lock, C.; Tsien, R. W.; Steinman, L. Inhibitory role for GABA in autoimmune inflammation. *Proc. Natl. Acad. Sci.* **2010**, *107*, 2580−2585.

(8) Alam, S.; Laughton, D. L.; Walding, A.; Wolstenholme, A. J. Human peripheral blood mononuclear cells express $GABA_A$ receptor subunits. *Mol. Immunol.* **2006**, *43*, 1432−1442.

(9) Mendu, S. K.; Bhandage, A.; Jin, Z.; Birnir, B. Different subtypes of GABA-A receptors are expressed in human, mouse and rat T lymphocytes. *PLoS One* **2012**, *7*, No. e42959.

(10) Kanatani, S.; Fuks, J. M.; Olafsson, E. B.; Westermark, L.; Chambers, B.; Varas-Godoy, M.; Uhlén, P.; Barragan, A. Voltage-dependent calcium channel signaling mediates $GABA_A$ receptor-induced migratory activation of dendritic cells infected by Toxoplasma gondii. *PLoS Pathog.* **2017**, *13*, e1006739−e1006768.

(11) Reyes-García, M. G.; Hernández-Hernández, F.; Hernández-Téllez, B.; García-Tamayo, F. GABA (A) receptor subunits RNA expression in mice peritoneal macrophages modulate their IL-6/IL-12 production. *J. Neuroimmunol.* **2007**, *188*, 64−68.

(12) Kim, J. K.; Kim, Y. S.; Lee, H.-M.; Jin, H. S.; Neupane, C.; Kim, S.; Lee, S.-H.; Min, J.-J.; Sasai, M.; Jeong, J.-H.; Choe, S.-K.; Kim, J.-M.; Yamamoto, M.; Choy, H. E.; Park, J. B.; Jo, E.-K. GABAergic signaling linked to autophagy enhances host protection against intracellular bacterial infections. *Nat. Commun.* **2018**, *9*, 4184.

(13) Tian, J.; Dang, H.; Karashchuk, N.; Xu, I.; Kaufman, D. L. A clinically applicable positive allosteric modulator of GABA receptors promotes human β-cell replication and survival as well as GABA's ability to inhibit inflammatory T cells. *J. Diabetes Res.* **2019**, *2019*, 5783545.

(14) Tian, J.; Chau, C.; Hales, T. G.; Kaufman, D. L. $GABA_A$ receptors mediate inhibition of T cell responses. *J. Neuroimmunol.* **1999**, *96*, 21−28.

(15) Yocum, G. T.; Turner, D. L.; Danielsson, J.; Barajas, M. B.; Zhang, Y.; Xu, D.; Harrison, N. L.; Homanics, G. E.; Farber, D. L.; Emala, C. W. $GABA_A$ receptor α4-subunit knockout enhances lung inflammation and airway reactivity in a murine asthma model. *Am. J. Physiol. Lung Cell Mol. Physiol.* **2017**, *313*, L406−L415.

(16) Neumann, S.; Boothman-Burrell, L.; Gowing, E. K.; Jacobsen, T. A.; Ahring, P. K.; Young, S. L.; Sandager-Nielsen, K.; Clarkson, A. N. The delta-subunit selective $GABA_A$ receptor modulator, DS2, improves stroke recovery via an anti-inflammatory mechanism. *Front. Neurosci.* **2019**, *13*, 1133.

(17) Sieghart, W.; Sperk, G. Subunit composition, distribution and function of $GABA_A$ receptor subtypes. *Curr. Top. Med. Chem.* **2002**, *2*, 795−816.

(18) Zheleznova, N. N.; Sedelnikova, A.; Weiss, D. S. Function and modulation of δ-containing $GABA_A$ receptors. *Psychoneuroendocrinology* **2009**, *34*, S67−S73.

(19) Johnston, G. A. R.; Chebib, M.; Hanrahan, J. R.; Mewett, K. N. $GABA_C$ receptors as drug targets. *Curr. Drug Targets: CNS Neurol. Disord.* **2003**, *2*, 260−268.

(20) Hinton, T.; Johnston, G. A. R. Antagonists of ionotropic receptors for the inhibitory neurotransmitter GABA: therapeutic indications. In *GABA and glutamate - new developments in neurotransmission research*; Samardzic, J., Ed.; IntechOpen: Serbia, 2018; Vol. *6*, pp. 91−105.

(21) Maramai, S.; Benchekroun, M.; Ward, S. E.; Atack, J. R. Subtype selective γ-aminobutyric acid type A receptor ($GABA_AR$) modulators acting at the benzodiazepine binding site: an update. *J. Med. Chem.* **2020**, *63*, 3425−3446.

(22) Krall, J.; Balle, T.; Krogsgaard-Larsen, N.; Sørensen, T. E.; Krogsgaard-Larsen, P.; Kristiansen, U.; Frølund, B. $GABA_A$ receptor partial agonists and antagonists: structure, binding mode, and pharmacology. *Adv. Pharmacol.* **2015**, 201−227.

(23) Heaulme, M.; Chambon, J.-P.; Leyris, R.; Molimard, J.-C.; Wermuth, C. G.; Biziere, K. Biochemical characterization of the interaction of three pyridazinyl-GABA derivatives with the $GABA_A$ receptor site. *Brain Res.* **1986**, *384*, 224−231.

(24) Krehan, D.; Storustovu, S. I.; Liljefors, T.; Ebert, B.; Nielsen, B.; Krogsgaard-Larsen, P.; Frølund, B. Potent 4-arylalkyl-substituted 3-isothiazolol $GABA_A$ competitive/noncompetitive antagonists: synthesis and pharmacology. *J. Med. Chem.* **2006**, *49*, 1388−1396.

(25) Johnston, G. A. Advantages of an antagonist: bicuculline and other GABA antagonists. *Br. J. Pharmacol.* **2013**, *169*, 328−336.

(26) Falk-Petersen, C. B.; Tsonkov, T. M.; Nielsen, M. S.; Harpsøe, K.; Bundgaard, C.; Frølund, B.; Kristiansen, U.; Gloriam, D. E.; Wellendorph, P. Discovery of a new class of orthosteric antagonists with nanomolar potency at extrasynaptic GABAA receptors. *Sci. Rep.* **2020**, *10*, 10078.

(27) Talele, T. T. Opportunities for tapping into three-dimensional chemical space through a quaternary carbon. *J. Med. Chem.* **2020**, *63*, 13291−13315.

(28) Hiesinger, K.; Dar'in, D.; Proschak, E.; Krasavin, M. Spirocyclic scaffolds in medicinal chemistry. *J. Med. Chem.* **2021**, *64*, 150−183.

(29) Carreira, E. M.; Fessard, T. C. Four-membered ring-containing spirocycles: synthetic strategies and opportunities. *Chem. Rev.* **2014**, *114*, 8257−8322.

(30) Zhu, S.; Noviello, C. M.; Teng, J.; Walsh, R. M., Jr.; Kim, J. J.; Hibbs, R. E. Structure of a human synaptic $GABA_A$ receptor. *Nature* **2018**, *559*, 67−72.

(31) Petersen, J. G.; Bergmann, R.; Krogsgaard-Larsen, P.; Balle, T.; Frølund, B. Probing the orthosteric binding site of $GABA_A$ receptors with heterocyclic GABA carboxylic acid bioisosteres. *Neurochem. Res.* **2014**, *39*, 1005−1015.

(32) Masiulis, S.; Desai, R.; Uchański, T.; Serna Martin, I.; Laverty, D.; Karia, D.; Malinauskas, T.; Zivanov, J.; Pardon, E.; Kotecha, A.; Steyaert, J.; Miller, K. W.; Aricescu, A. R. $GABA_A$ receptor signalling mechanisms revealed by structural pharmacology. *Nature* **2019**, *565*, 454−459.

(33) Chandra, D.; Halonen, L. M.; Linden, A.-M.; Procaccini, C.; Hellsten, K.; Homanics, G. E.; Korpi, E. R. Prototypic $GABA_A$ receptor agonist muscimol acts preferentially through forebrain high-affinity binding sites. *Neuropsychopharmacology* **2010**, *35*, 999−1007.

(34) Ebert, B.; Thompson, S. A.; Saounatsou, K.; McKernan, R.; Krogsgaard-Larsen, P.; Wafford, K. A. Differences in agonist/antagonist binding affinity and receptor transduction using recombinant human γ-aminobutyric acid type A receptors. *Mol. Pharmacol.* **1997**, *52*, 1150−1156.

(35) Frølund, B.; Jensen, L. S.; Guandalini, L.; Canillo, C.; Vestergaard, H. T.; Kristiansen, U.; Nielsen, B.; Stensbøl, T. B.; Madsen, C.; Krogsgaard-Larsen, P.; Liljefors, T. Potent 4-aryl- or 4-arylalkyl-substituted 3-isoxazolol $GABA_A$ antagonists: synthesis, pharmacology, and molecular modeling. *J. Med. Chem.* **2005**, *48*, 427−439.

(36) Krall, J.; Bavo, F.; Falk-Petersen, C. B.; Jensen, C. H.; Nielsen, J. O.; Tian, Y.; Anglani, V.; Kongstad, K. T.; Piilgaard, L.; Nielsen, B.;

https://doi.org/10.1021/acs.jmedchem.1c00290
J. Med. Chem. XXXX, XXX, XXX−XXX

Gloriam, D. E.; Kehler, J.; Jensen, A. A.; Harpsøe, K.; Wellendorph, P.; Frølund, B. Discovery of 2-(imidazo[1,2-b]pyridazin-2-yl)acetic acid as a new class of ligands selective for the γ-hydroxybutyric acid (GHB) high-affinity binding sites. *J. Med. Chem.* **2019**, *62*, 2798−2813.

(37) Hansen, S. B.; Sulzenbacher, G.; Huxford, T.; Marchot, P.; Taylor, P.; Bourne, Y. Structures of Aplysia AChBP complexes with nicotinic agonists and antagonists reveal distinctive binding interfaces and conformations. *EMBO J.* **2005**, *24*, 3635−3646.

(38) Terejko, K.; Kaczor, P. T.; Michałowski, M. A.; Dąbrowska, A.; Mozrzymas, J. W. The C loop at the orthosteric binding site is critically involved in GABAA receptor gating. *Neuropharmacology* **2020**, *166*, 107903.

(39) Giraudo, A.; Krall, J.; Nielsen, B.; Sørensen, T. E.; Kongstad, K. T.; Rolando, B.; Boschi, D.; Frølund, B.; Lolli, M. L. 4-Hydroxy-1,2,3-triazole moiety as bioisostere of the carboxylic acid function: a novel scaffold to probe the orthosteric γ-aminobutyric acid receptor binding site. *Eur. J. Med. Chem.* **2018**, *158*, 311−321.

(40) Giraudo, A.; Krall, J.; Bavo, F.; Nielsen, B.; Kongstad, K. T.; Rolando, B.; De Blasio, R.; Gloriam, D. E.; Löffler, R.; Thiesen, L.; Harpsøe, K.; Frydenvang, K.; Boschi, D.; Wellendorph, P.; Lolli, M. L.; Jensen, A. A.; Frølund, B. Five-membered N-heterocyclic scaffolds as novel amino bioisosteres at γ-aminobutyric acid (GABA) type A receptors and GABA transporters. *J. Med. Chem.* **2019**, *62*, 5797−5809.

(41) Krall, J.; Jensen, C. H.; Sørensen, T. E.; Nielsen, B.; Jensen, A. A.; Sander, T.; Balle, T.; Frølund, B. Exploring the orthosteric binding site of the γ-aminobutyric acid type A receptor using 4-(piperidin-4-yl)-1-hydroxypyrazoles 3- or 5-imidazolyl substituted: design, synthesis, and pharmacological evaluation. *J. Med. Chem.* **2013**, *56*, 6536−6540.

(42) Berezhnoy, D.; Gravielle, M. C.; Farb, D. H. Pharmacology of the $GABA_A$ receptor. In *Handbook of Contemporary Neuropharmacology*; Sibley, D. R; Hanin, I.; Kuhar, M.; Skolnick, P., Eds., John Wiley & Sons, Inc., 2007.

(43) Sander, T.; Frølund, B.; Bruun, A. T.; Ivanov, I.; McCammon, J. A.; Balle, T. New insights into the $GABA_A$ receptor structure and orthosteric ligand binding: receptor modeling guided by experimental data. *Proteins: Struct., Funct., Bioinf.* **2011**, *79*, 1458−1477.

(44) Møller, H. A.; Sander, T.; Kristensen, J. L.; Nielsen, B.; Krall, J.; Bergmann, M. L.; Christiansen, B.; Balle, T.; Jensen, A. A.; Frølund, B. Novel 4-(piperidin-4-yl)-1-hydroxypyrazoles as γ-aminobutyric $acid_A$ receptor ligands: synthesis, pharmacology, and structure−activity relationships. *J. Med. Chem.* **2010**, *53*, 3417−3421.

(45) Frølund, B.; Jørgensen, A. T.; Tagmose, L.; Stensbøl, T. B.; Vestergaard, H. T.; Engblom, C.; Kristiansen, U.; Sanchez, C.; Krogsgaard-Larsen, P.; Liljefors, T. Novel class of potent 4-arylalkyl substituted 3-isoxazolol $GABA_A$ antagonists: synthesis, pharmacology, and molecular modeling. *J. Med. Chem.* **2002**, *45*, 2454−2468.

(46) Frølund, B.; Tagmose, L.; Liljefors, T.; Stensbøl, T. B.; Engblom, C.; Kristiansen, U.; Krogsgaard-Larsen, P. A novel class of potent 3-isoxazolol $GABA_A$ antagonists: design, synthesis, and pharmacology. *J. Med. Chem.* **2000**, *43*, 4930−4933.

(47) Frølund, B.; Jensen, L. S.; Storustovu, S. I.; Stensbøl, T. B.; Ebert, B.; Kehler, J.; Krogsgaard-Larsen, P.; Liljefors, T. 4-Aryl-5-(4-piperidyl)-3-isoxazolol $GABA_A$ antagonists: synthesis, pharmacology, and structure−activity relationships. *J. Med. Chem.* **2007**, *50*, 1988−1992.

(48) Spurny, R.; Debaveye, S.; Farinha, A.; Veys, K.; Vos, A. M.; Gossas, T.; Atack, J.; Bertrand, S.; Bertrand, D.; Danielson, U. H.; Tresadern, G.; Ulens, C. Molecular blueprint of allosteric binding sites in a homologue of the agonist-binding domain of the α7 nicotinic acetylcholine receptor. *Proc. Natl. Acad. Sci.* **2015**, *112*, E2543−E2552.

(49) Boileau, A. J.; Newell, J. G.; Czajkowski, C. $GABA_A$ receptor β_2 Tyr^{97} and Leu^{99} line the GABA-binding site. Insights into mechanisms of agonist and antagonist actions. *J. Biol. Chem.* **2002**, *277*, 2931−2937.

(50) Wagner, D. A.; Czajkowski, C.; Jones, M. V. An arginine involved in GABA binding and unbinding but not gating of the $GABA_A$ receptor. *J. Neurosci.* **2004**, *24*, 2733−2741.

(51) Uhlén, M.; Fagerberg, L.; Hallström, B. M.; Lindskog, C.; Oksvold, P.; Mardinoglu, A.; Sivertsson, Å.; Kampf, C.; Sjöstedt, E.; Asplund, A.; Olsson, I.; Edlund, K.; Lundberg, E.; Navani, S.; Szigyarto, C. A.-K.; Odeberg, J.; Djureinovic, D.; Takanen, J. O.; Hober, S.; Alm, T.; Edqvist, P.-H.; Berling, H.; Tegel, H.; Mulder, J.; Rockberg, J.; Nilsson, P.; Schwenk, J. M.; Hamsten, M.; von Feilitzen, K.; Forsberg, M.; Persson, L.; Johansson, F.; Zwahlen, M.; von Heijne, G.; Nielsen, J.; Pontén, F. Tissue-based map of the human proteome. *Science* **2015**, *347*, 1260419.

(52) Sparrow, E. L.; James, S.; Hussain, K.; Beers, S. A.; Cragg, M. S.; Bogdanov, Y. D. Activation of GABA(A) receptors inhibits T cell proliferation. *PLoS One* **2021**, *16*, No. e0251632.

(53) Falk-Petersen, C. B.; Søgaard, R.; Madsen, K. L.; Klein, A. B.; Frølund, B.; Wellendorph, P. Development of a robust mammalian cell-based assay for studying recombinant $\alpha_4\beta_{1/3}\delta$ $GABA_A$ receptor subtypes. *Basic Clin. Pharmacol. Toxicol.* **2017**, *121*, 119−129.

(54) Risgaard, R.; Ettrup, A.; Balle, T.; Dyssegaard, A.; Hansen, H. D.; Lehel, S.; Madsen, J.; Pedersen, H.; Püschl, A.; Badolo, L.; Bang-Andersen, B.; Knudsen, G. M.; Kristensen, J. L. Radiolabelling and PET brain imaging of the α1-adrenoceptor antagonist Lu AE43936. *Nucl. Med. Biol.* **2013**, *40*, 135−140.

(55) *Schrödinger Release 2019−4: LigPrep*; Schrödinger, LLC: New York, NY, 2019.

(56) Madhavi Sastry, G.; Adzhigirey, M.; Day, T.; Annabhimoju, R.; Sherman, W. Protein and ligand preparation: parameters, protocols, and influence on virtual screening enrichments. *J. Comput.-Aided Mol. Des.* **2013**, *27*, 221−234.

(57) Sherman, W.; Day, T.; Jacobson, M. P.; Friesner, R. A.; Farid, R. Novel procedure for modeling ligand/receptor induced fit effects. *J. Med. Chem.* **2006**, *49*, 534−553.

(58) Friesner, R. A.; Murphy, R. B.; Repasky, M. P.; Frye, L. L.; Greenwood, J. R.; Halgren, T. A.; Sanschagrin, P. C.; Mainz, D. T. Extra precision glide: docking and scoring incorporating a model of hydrophobic enclosure for protein−ligand complexes. *J. Med. Chem.* **2006**, *49*, 6177−6196.

(59) Halgren, T. A. Identifying and characterizing binding sites and assessing druggability. *J. Chem. Inf. Model.* **2009**, *49*, 377−389.

(60) Hussain, K.; Hargreaves, C. E.; Roghanian, A.; Oldham, R. J.; Chan, H. T. C.; Mockridge, C. I.; Chowdhury, F.; Frendéus, B.; Harper, K. S.; Strefford, J. C.; Cragg, M. S.; Glennie, M. J.; Williams, A. P.; French, R. R. Upregulation of FcγRIIb on monocytes is necessary to promote the superagonist activity of TGN1412. *Blood* **2015**, *125*, 102−110.

https://doi.org/10.1021/acs.jmedchem.1c00290
J. Med. Chem. XXXX, XXX, XXX−XXX